CHALMERS
UNIVERSITY OF TECHNOLOGY

Corrosion risks in co-processing of rapeseed oil

A study on degradation of triglycerides and its relation to risk of corrosion

Master's thesis in Material Chemistry

AMANDA MÅRTENSSON

Department of Chemistry and Chemical Engineering
Chalmers University of Technology
Gothenburg, Sweden 2020

Master's thesis 2020

Corrosion risks in processing of rapeseed oil

A study on degradation of triglycerides and its relation to risk of corrosion

AMANDA MÅRTENSSON

CHALMERS
UNIVERSITY OF TECHNOLOGY

Department of Chemistry and Chemical Engineering
Division of Material Chemistry
Chalmers University of Technology
Gothenburg, Sweden 2020

Corrosion risks in co-procesessing of rapeseed oil
A study on degradation of triglycerides and its relation to risk of corrosion
AMANDA MÅRTENSSON

© AMANDA MÅRTENSSON 2020.

Supervisor: Mats Hörnfelt, Preem AB
Examiner: Jesper Liske, Department of Chemistry and Chemical Engineering

Master's Thesis 2020
Department of Chemistry and Chemical Engineering
Division of Material Chemistry
Chalmers University of Technology
SE-412 96 Gothenburg

Cover: Crops of rape. Photo taken by Amanda Mårtensson.

Gothenburg, Sweden 2020

Corrosion risks in co-processing of rapeseed oil
A study on degradation of rapeseed oil and its relation to risk of corrosion
AMANDA MÅRTENSSON
Department of Chemistry and Chemical Engineering
Chalmers University of Technology

Abstract

With an increased knowledge about greenhouse gas emissions and climate change, the interest in renewable energy sources are increasing remarkably. At Preem's refinery in Lysekil an ongoing project is the refining of a more renewable diesel by initially adding 2 - 10 wt% of rapeseed oil into the already present Synergetic Saturation (SynSat) unit. The added rapeseed oil is blended in with fossil oil in a so called co-processing technique.

Rapeseed oil consists of triglycerides, which in turns consists of different types of fatty acids which can cause fatty acid corrosion. This occurs when triglycerides decompose into free fatty acids. This master thesis investigated the decomposition of triglycerides at temperatures of 290, 310 and 330 °C together with a mixture of 5, 10, 15 and 100 wt% of rapeseed oil for each temperature. The pressure was set to 59 bar and LHSV to 1.5 h^{-1} in hydrogen atmosphere. TAN values concluded that none of the samples caused a risk of corrosion. By comparing the TAN values with a theoretical chemical kinetic model over degradation of vegetable oil in a hydrogen free environment it was concluded that the presence of hydrogen gas is of great importance. All samples tested in a hydrogen environment showed a TAN value of < 3 mg KOH/g whereas all theoretical samples in a hydrogen free environment gave a TAN value of > 39 mg KOH/g.

With time an increase in added amount of rapeseed oil into the SynSat unit is planned to 20 wt% or more. Since vegetable oils contains much more chlorides than fossil oil there is a risk of deposition of NH_4Cl in the upstream system of the revamped SynSat unit, which can cause fouling or corrosion in pipes of heat exchanger or air coolers. Calculations in combination with published diagrams showed that there in fact is a risk of NH_4Cl salt deposition in the upstream system of the SynSat unit. Therefore an water injection point is necessary at this stream to avoid such deposition.

The degradation of rapeseed oil forms unwanted by-products like CO_2, which in contact with water is corrosive. Other products such as H_2S and NH_3 are formed as well in the process. The addition of an water injection point to avoid salt deposition of NH_4Cl, can therefore cause sweet or sour corrosion in the amine recovery system. When investigating the system it showed to be of sour corrosion dominating type, where a risk of corrosion was found to be possible in some streams. It was however not possible to predict the type of corrosion or corrosion rate of such a system due to the complicated reaction mechanisms of sour corrosion.

Keywords: rapeseed oil, free fatty acids, co-processing, sweet corrosion, sour corrosion, ammonium salt, oil refinery, TAN

Acknowledgements

I would like to thank my supervisor at Preem, Mats Hörnfelt, for making this project possible. From the request of writing my master thesis at Preem in March last year until today he has supported me and found new interesting ways to make this project possible. Without Mats this master thesis would not have been what it is today.

I would also like to thank both Anders Balksten and Joakim Lindén for all the support during this year. I have come with a lot of different questions and reflections which you always tried to help me with, getting to an answer. Especially thanks to Anders for helping me finding new ways to look at problems when I had found myself stuck. For Joakim, I would want to especially thank you for your expertise in the subject which has helped me a lot in this master thesis.

Finally, I would like to thank my patient and supporting partner Viktor, who has not only cheered for me but also supported me in all ways possible during this year.

Amanda Mårtensson, Gothenburg, May 2020

Abbreviations

ASS	Austenitic Stainless Steel
CFPP	Cold Filter Plugging Point
CHPS	Cold High Pressure Separator
CLP	Cloud Point
FA	Fatty Acid
FFA	Free Fatty Acid
GC	Gas Chromatography
GHG	Green House Gases
HDA	Hydrodearomatization
HDC	Hydrodecarboxylation
HDO	Hydrodeoxygenation
HDS	Hydrodesulfurization
HHPS	Hot High Pressure Separator
HIC	Hydrogen Induced Cracking
HPLC	High Performance Liquid Chromatography
HS	High Sulfur
KERO	Kerosene
LAGO	Light Atmospheric Gas Oil
LHSV	Liquid Hourly Space Velocity
LS	Low Sulfur
NA	Naphthenic Acid
NMR	Nuclear Magnetic Resonance
SCC	Stress Cracking Corrosion
SynSat	Synergetic Saturation
TAG	Triglyceride
TAN	Total Acid Number

Contents

List of Figures

List of Tables

1 Introduction

Due to the increased knowledge about climate change, its influence by greenhouse gas (GHG) emissions together with diminished oil sources, renewable fuels are of great interest on the market today. [1] Combustion of fossil transportation fuels causes a momentous part of the overall CO_2 emissions, which can be directly related to greenhouse gas emissions and hence increased global warming. Therefore, research for carbon neutral technologies are being developed and improved. [2] One potential green energy source providing less environmental impact in comparison to fossil fuel is renewable diesel fuel derived from vegetable oils.

1.1 Background

When producing renewable diesel fuel, vegetable oil can be used either by solely adding it or by blending the vegetable oil with petroleum oil in a present hydroprocessing unit, so called co-processing. [3, 4] In 2011 Preem's Evolution Diesel was released on the market where tall oil is co-processed with light atmospheric gasoil (LAGO). Now a new expansion in Preem's refinery located Lysekil is planned, where LAGO will be co-processed together with rapeseed oil. Initially 2 - 10 wt% will be co-processed but within a future of a few years, this will be increased to 20 wt% or more. The production of this partially renewable diesel will be produced in a revamped synergetic saturation (SynSat) unit which today produces diesel.

The new revamped design will have rapeseed oil mixed together with LAGO before entering the first unit reactor. However, while designing the new renewable feed system into the current design, several aspects have to be further investigated. Some of these aspects are the high oxygen content, immiscibility with fossil fuel and high viscosity of vegetable oil. Therefore, the rapeseed oil has to be processed before being used as diesel fuel. [1, 5] These reactions are performed in the unit reactors where hydrogen gas and catalyst will hydrotreat the compounds in the vegetable oil, forming hydrocarbons similar to the ones in fossil diesel. These reactions are known as hydrodeoxygenation (HDO) and hydrodecarboxylation (HDC). [6]

Another aspect is that all vegetable oils consist of triglycerides which in turn consists of different fatty acids. [6] Due to the free fatty acids and high concentrations of organic oxygenates in vegetable oil, corrosion issues in storage tanks and feed lines will be increased in comparison to petroleum oils. [6, 7, 8] The risk of corrosion can be measured by the

Total Acid Number (TAN) which represents the degree of oxidation and hydrolysis in a feedstock which can be related to its corrosion. [3] No previous studies regarding a summary of TAN for rapeseed oil at different temperatures and wt% of renewable feed have been found in literature.

According to Preems internal calculations, a larger portion of chlorides is to be expected when adding rapeseed oil into the SynSat unit. With an increased amount of chlorides, a possible deposition of NH_4Cl at heat exchangers or air coolers can occur at normal operating temperatures where there previously was no salt deposition. [9] The risk of ammonium corrosion must therefore be investigated further.

One common way to reduce the risk of salt deposition is to add a water injection point into the feed systems where deposition of salt can occur. [10] This addition of water may however cause sour or sweet corrosion when coming in contact with H_2S and/or CO_2. [11] Carbon dioxide is a by-product of hydrocarboxylation when co-processing rapeseed oil with fossil fuel and was not present before the revamp of the SynSat unit. [4, 12] Therefore such risk of corrosion must be investigated in the project of the SynSat unit revamp.

1.2 Aim

This master thesis aims to investigate three possible causes of corrosion when co-processing rapeseed oil in a hydrotreating unit at Preems refinery in Lysekil. Free fatty acid corrosion, ammonium salt corrosion and sour and sweet corrosion will be investigated with focus being laid on the risk of corrosion and material durability. The master thesis will also cover the degradation of triglycerides into free fatty acids at different temperatures and mixtures. This by finding possible correlations between the decomposition of triglycerides and risk of corrosion of the material in the processing unit. For corrosion investigations on the amine recovery system of the SynSat unit this master thesis aims to find a reliable and well applicable prediction model of corrosion together with analyzing the risk of deposition of ammonium salts due to water injections.

1.3 Limitations

In such a complex system as a refinery several possible corrosion aspects has to be taken in consideration as a whole. However in this master thesis the focus has been laid on fatty acid, aqueous and ammonium salt corrosion since these are some the most probable corrosion after co-processing the current feed of LAGO with rapeseed oil.

Different crude oils do have a significant difference in corrosivity. But since that would cause too high of a workload to investigate all possible crude oils running through the refinery, only one will be covered in this master thesis. There are several methods measuring the corrosivity of a crude oil. Analyzing Total Acid Number (TAN) is one of the most common methods, which will be used in this thesis. [13]

When using corrosion prediction models there are many variables that has to be taken

into consideration. Therefore one have to decide which of these variables that are of most importance to the system of interest.

One last limitation in this master thesis is that it does not account for wall shear stress, velocity or other flow impacts of the feed inside the pipes when measuring the corrosivity.

2 Theory

2.1 Rapeseed oil

Rapeseed oil originates from the *Brassica* plant and is the third largest produced vegetable oil globally after palm- and soybean oil. [14] Rapeseed can germinate at low temperatures, making it accessible also in the northern parts of the globe. [15] Due to its accessibility and preferable characteristics, rapeseed oil is a popular choice when co-processing renewable feed. Because of the reasons described above, rapeseed oil is also the choice for the revamped SynSat unit of Preems' refinery in Lysekil.

Rapeseed oil is high in content of monounsaturated fatty acids (58%), but it also contains polyunsaturated fatty acids (33%) and saturates (9%). [16] In general, vegetable oils as fuel components yield less CO and CO_2 emissions. [15] Vegetable oil, as all biomass materials, consist of high amounts of chlorides whereas the amount of sulfur is low. [17]

2.1.1 Triglycerides in rapeseed oil

The main components in rapeseed oil, as in all vegetable oils, are made up of carbon, oxygen and hydrogen. Through various combinations, these atoms form different variants of triglycerides (TAGs) which represent 96 - 98% of the oil composition. [18] TAGs are composed of three fatty acids (FAs) esterified to a glycerol molecule. [6, 18] An example of a triglyceride structure is given in Figure 2.1. It is the fatty acids, and the chemical structure of its glycerol molecule that determine the properties and characteristics of the triglyceride. [19] The fatty acids can vary in both carbon chain length and saturation levels, and the number of double bonds determines the heat stability of the oil product. [14] At lower temperatures, fatty acids can be seen as rather harmless oils. However, at higher temperatures, as in the SynSat unit, fatty acids may cause severe corrosion of steel. [20]

In rapeseed oil, the fatty acid molecules mainly consist of chains with 18 to 22 carbon atoms. [6] All fatty acids present in the rapeseed oil are given in Table 2.1. The number behind the fatty acid represents the number of carbons in the hydrocarbon chain and the second number represents the amount of double bonds in the fatty acid.

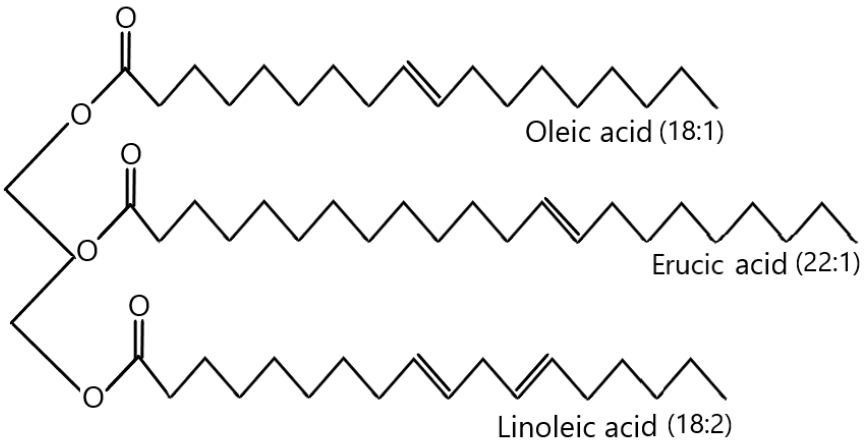

Figure 2.1: *An example of a triglyceride structure.*

Oleic acid, which represent more than 61% of the fatty acids in rapeseed oil, is an unsaturated fatty acid with a backbone of 18 carbons. Oleic acid occurs naturally in both animal fats as well as in vegetable oils. [21] An example of an oleic acid can be seen in Figure 2.1. The second largest contribution to the rapeseed oil composition is linoleic acid. Linoleic acid is a polyunsaturated fatty acid with doulbe bonds on the 9th and 12th carbon and can be seen in Figure 2.1. [22] Linolenic acid is also a polyunsaturated fatty acid and is the third largest component in terms of weight percent and consists of three double bonds. [23] All of the three dominating fatty acids are thus of unsaturated type. From Table 2.1 an absence of free fatty acids (FFA) can be observed. [2] Free fatty acids are fatty acids which have been separated from the triglyceride molecule. [18] To transform a double bonded carbon chain of a free fatty acid into a linear carbon-carbon chain, a higher hydrogen gas consumption is required, causing higher operating costs. [2]

Table 2.1: *Composition of fatty acids in commercial rapeseed oil.* [24]

Fatty acid content	**Molecular Formula**	**Total** (wt%)	**C** (wt%)	**H** (wt%)	**O** (wt%)
Stearic (18:0)	$C_{18}H_{36}O_2$	7	5.4	0.9	0.8
Oleic (18:1)	$C_{18}H_{34}O_2$	61.1	46.9	7.4	7.0
Linoleic (18:2)	$C_{18}H_{32}O_2$	20.9	16.1	2.2	2.4
Linolenic (18:3)	$C_{18}H_{30}O_2$	9.1	7.0	0.9	1.0
Gadoleic (20:1)	$C_{20}H_{30}O_2$	1.4	1.2	0.1	0.2
Erucic (22:1)	$C_{22}H_{32}O_2$	0.5	0.5	0.1	0.1
Calculated (wt%)		100	77.0	11.6	11.4
Analyzed (wt%)	Error = max. $\pm 0.5\%$		77.1	11.8	11.1

2.2 SynSat Unit

The SynSat unit is a process plant which removes sulfur - and aromatic compounds from hydrocarbons with hydrogen gas and a reactor mass. The feed running through the unit is either kerosene (KERO) or light atmospheric gasoil (LAGO). It is characterized by its two in-series-reactors called HDS and HDA reactors. The unit can operate in two modes; hydrodesulfurization (HDS) where removal of sulfur occur, and hydroaromatization (HDA) which removes both sulfur- and aromatic compounds. Between the two reactors is an interstage stripper which separates light hydrocarbons and H_2S since the HDA reactor cannot handle sulphur. The unit also includes an amine recovery system, which separates the formed NH_3 from the gas. Together with a stripping system, performing after-treatment of the reactor liquid products in order to obtain desirable properties of the product feed. A simplified scheme of the SynSat unit is shown in Figure 2.2.

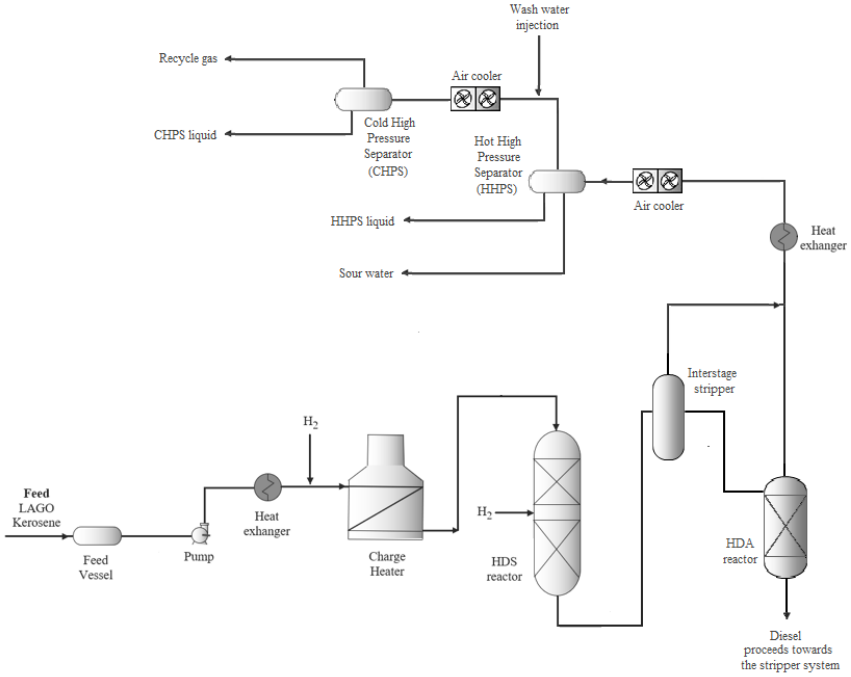

Figure 2.2: *Simplified scheme of the present SynSat unit.*

Hydrotreating is a catalytic chemical process where unstable molecules, for example components of oxygen, nitrogen and sulfur, are refined. These components will react with the added hydrogen gas inside the reactor forming H_2O and the corrosive compounds of H_2S and NH_3. [25] By these reactions sulfur is removed by 95 - 99%+. Some of the purposes of hydrotreating petroleum oil are to reduce the sulfur content and enhance the cetane number. Even in low concentrations sulfur can poison the catalyst in the HDA reactor which is one reason for desired removal. In addition to this, saturation of chemical compounds, such as aromatics or naphthenes preferably occurs. [26]

The current feedstock of either KERO or LAGO flows from tanks into the SynSat unit where it passes a feed vessel and thereafter a heater, where hydrogen gas is introduced. The stream temperature of the outgoing oven equals the inlet temperature into the HDS reactor. The reactor consists of two beds filled with catalysts of nickel, molybdenum and phosphorous oxides reacting with the passing feed transforming it to linear hydrocarbons. Between the first and second bed, hydrogen gas is added via quenching in order to replenish the hydrogen used for reactions in the first bed, making further hydrodesulfurization possible. When running both the HDS- and the HDA reactor, the reactor gas product is flowing towards the amine absorber system. Here the gas is condensed and H_2S-rich gas is separated from the liquid. The gas then flows into the amine absorber tower, where an amine flow absorbs the H_2S and then goes to the amine recovery. The reactor liquid product proceeds towards the stripper section in order to obtain the desired product properties.

2.2.1 Revamped SynSat Unit

In the revamped SynSat unit, an additional mode will be added where initially 2 - 10 wt% of rapeseed oil, added via a quill, will be co-processed with LAGO. A quill is a pipe consisting of slots or holes, mixing the renewable feed more easily with the LAGO stream. [27] Current material to the feed pipes is stainless steel alloy 321, which can be read about further in section 2.7.1. In the new revamped feed system, the rapeseed oil will be injected just before the inlet of the HDS reactor. This is to avoid corrosion risks earlier in the feed line due to free fatty acid formation from the heated rapeseed oil. [20] A simplified scheme of the planned additional feed of rapeseed oil is shown in Figure 2.3.

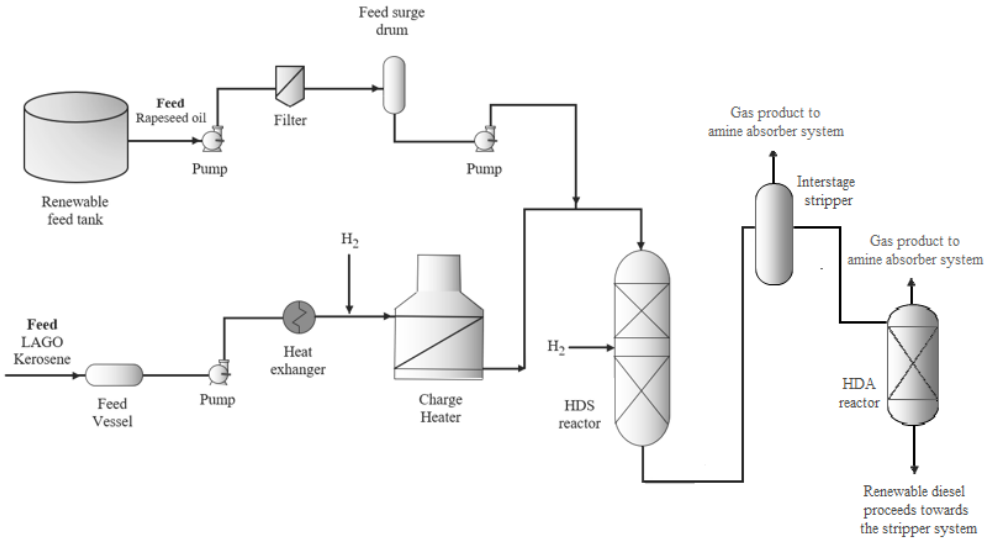

Figure 2.3: *Design prototype of renewable feed added to the petroleum feed stock.*

In Figure 2.4, the quill planned to be used for injection of rapeseed oil into the SynSat system is shown.

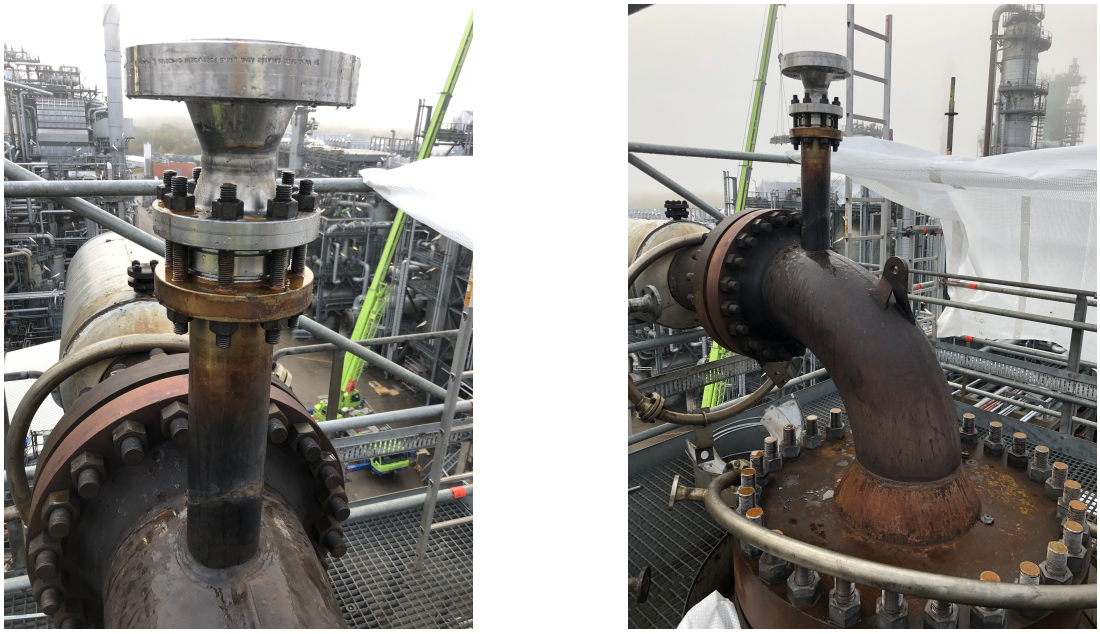

Figure 2.4: *The installed quill and inlet point of the SynSat unit. Photography by Preem.*

In the amine absorber system some rebuilding will be done as well, to prepare for the case where 20 wt% or more of rapeseed oil is planned to be co-processed with LAGO. The main difference in comparison with the unit before the revamp is the addition of another wash water injection point before the hot high pressure separator (HHPS), shown in Figure 2.5. This due to avoid fouling of ammonium chloride (NH_4Cl) and ammonium bisulfide (NH_4HS) on the pipes in heat exchangers and/or air coolers. [10]

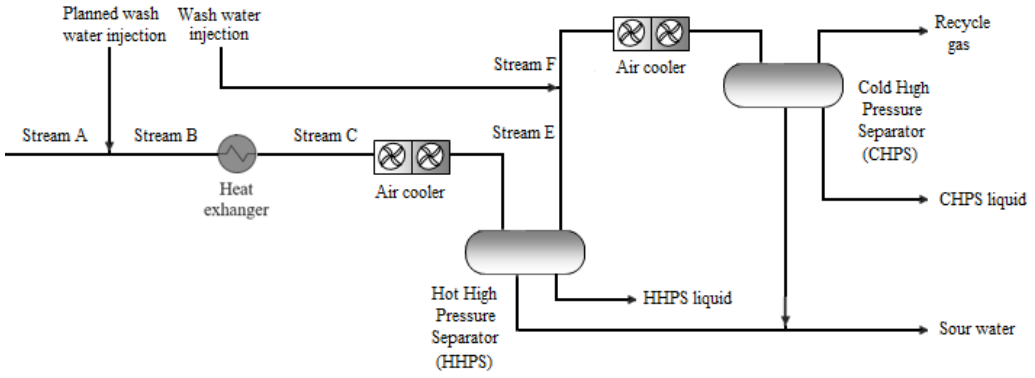

Figure 2.5: *Design scheme of initial parts of the amine recovery system.*

2.2.2 Light gas oil

Distillation products from the crude unit at Preems' refinery in Lysekil can be separated into six main fractions; fuel gas (< C2), liquefied petroleum gas (LPG, C3 and C4), naphtha, KERO, light and heavy atmospheric gasoil and atmospheric residue. Fuel, being the lightest fraction, comes out via the top whereas atmospheric residue, being the heaviest fraction, comes out via the bottom the crude distillation tower. In the current SynSat unit the feedstock varies between KERO and LAGO. It is however only LAGO that will be used as fossil feed when co-processing rapeseed oil after the revamp.

LAGO consists of hydrocarbons with 75% being saturated molecules of alkenes (n-paraffins), alkanes (iso-paraffins) and cyclo-alkanes (naphthenes), seen in Figure 2.6. [28] The remaining 25% composition represent aromatic hydrocarbons, such as toluene. Depending on the different chemical structures of the hydrocarbons, the flow properties of the final product can vary. [28, 29]

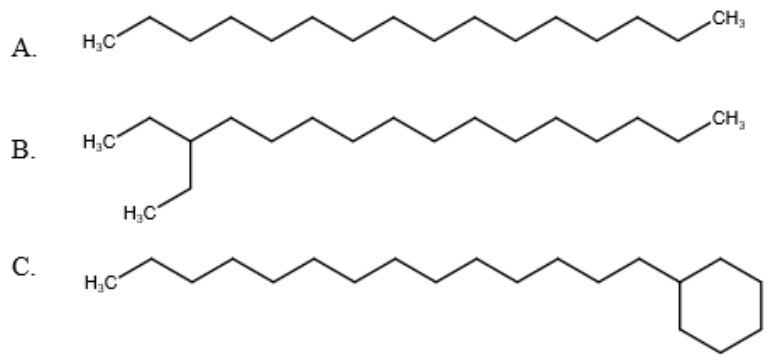

Figure 2.6: ***A.****Normal paraffin* ***B.*** *Branched (ISO) paraffin* ***C.*** *Cyclohexyl paraffin, also named naphthene.*

2.3 Co-processing rapeseed oil

One major advantage with the co-processing technology is the opportunity to use already existing units and technologies, reducing the capital costs. [30, 31] The reaction between the co-processed feed will occur in the already present reactors together with catalyst mass and an addition of hydrogen gas environment. Hydrotreating co-processed feed in the unit has the purpose of producing linear hydrocarbons compatible with the ones in diesel and to fulfill all specifications required in the finished diesel product. [6] This is done by transforming the double bonds in the fatty acids into saturated single carbon-carbon bonds by hydrogenation. The esters linkage is then separated, yielding one propane molecule and three molecules of saturated fatty acids. The final hydrocarbons are then formed by deoxidizing the fatty acid molecules. [32]

Co-processing vegetable oil with petroleum oil does come with several challenges. Firstly, biomass based diesel contains a noticeable amount of oxygen and other contaminants

which can cause rapid pressure drop build-up or deactivation of catalyst. Secondly, very exothermic reactions will occur and a larger amount of circulated, cleaned hydrogen gas, so called make-up gas is required for quenching. Therefore, the hydrogen balance in the refinery must be controlled, which might give a smaller unit capacity then during processing of petroleum. Due to the above described challenges, co-processing renewable feedstock with petroleum oil usually limits around 5 vol-%. In addition, co-processing vegetable oil containing a high amount of free fatty acids increases risk of severe corrosion in pipes and upstream equipment of the reactor. [6]

The main theory for occurrence of corrosion after the revamp are around two parts of the unit. Firstly, the quill, where the rapeseed oil is injected to mix with LAGO. This theory is primarily based on the high concentration of fatty acid in rapeseed oil which is known to cause corrosion. [6] The second part is in the pipes between the air cooler and the cold high pressure separator (CHPS) in the amine absorber system, due to the addition of wash water. In this part of the unit, acid components as H_2S and CO_2 may cause corrosion on the pipe steel material.

Initially the amount of co-processed rapeseed oil is set to 2 - 10 wt% but within some years the share of rapeseed oil is planned to be increased to 20 wt% or more. Therefore with an increased amount of rapeseed oil, higher free fatty acids concentrations and formation of CO_2 can be present in the feed causing corrosion.

In a study made by Walendziewski *et al.* 10 wt% and 20 wt% rapeseed oil where mixed with a balance of diesel under hydrogen gas with an operating pressure of 5 MPa and a temperature of 320 °C. LHSV was set to 2 h^{-1}. Used catalyst was $NiMo/Al_2O_3$. The study presented a hypothesis that the hydrogenolysis of ester bonds and hydrogenation of olefinic bonds in vegetable oils is the main reaction when co-processing. [33] Most interesting in this study with respect to the aim of this master thesis is the given acid number (mg KOH/g) which can be seen in Table 2.2. Here one can observe a rather large increase in acid number between the different mixtures of rapeseed oil. It is however important to remember that different crude oils can give different values of TAN.

Table 2.2: *Hydroprocessed mixture of 10 wt% and 20 wt% rapeseed oil at 320 °C.* [33]

Feedstock	10 wt%	20 wt%
Acid number [mg KOH/g]	0.6	1.74

Another study made by Zeuthen and Rasmussen describe how triglycerides in rapeseed oil reacts under hydroprocessing conditions with a 25 vol-% of renewable feed stock. The results showed that four different kinds of paraffin were formed with carbon backbones of 17, 18, 21 and 22 respectively. [6]

2.3.1 Degradation of rapeseed oil

The reaction pathway for degradation of triglycerides occurs by hydrogenation over a metal catalyst in two main steps, HDO and HDC, see Figure 2.7. The final products from both reactions are hydrocarbons together with by-products of linear n-alkenes, H_2O, CO

and CO_2. [4, 12] In the HDO step, hydrogen gas is added, forming linear n-alkanes. The main by-products are oxygen-containing groups, such as H_2O. HDO is a very hydrogen-consuming process with the amount of hydrogen required depending on type of vegetable oil and reaction pathway. [4]

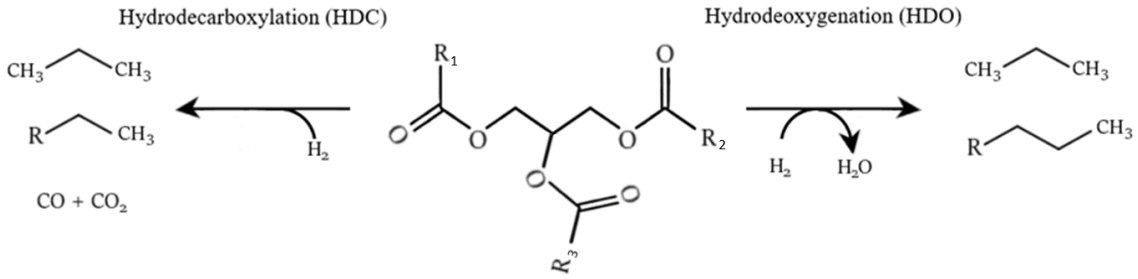

Figure 2.7: *Hydrogenation reactions of triglycerides.*

There are several similarities between HDO and the current HDS reaction at the SynSat unit. Comparing the two processes, both use hydrogen gas in order to eliminate oxygen and sulfur. One organic and one aqueous phase will be formed as products. The two processes also use similar catalyst and have the same process conditions with a high operating pressure. [34]

The formed hydrocarbon chain in HDC have one less carbon atom than in the fatty acid chain and main by-products are CO, CO_2 and propane. [4] Commonly the product consists of linear hydrocarbons although it can differ depending on the saturation level of the fatty acid in the original feedstock. A saturated feed will experience transformation to alkenes described in the sections of HDO and HDC above. Unsaturated feedstocks, however, will transform to only a smaller amount of shorter-chained alkenes. [4] The desirable reaction out of the two is HDO since HDC loses one carbon in order to form CO_2 and CO.

2.4 Cold flow properties

One of the main disadvantages of co-processing vegetable oil is its poor cold properties including low-temperature flow properties and high cloud point (CLP). CLP depends on the saturation level of fatty acids. A higher degree of unsaturated fatty acids gives a higher CLP than for saturates. CLP is the temperature where the liquid sample becomes cloudy due to formation of crystals. The crystals, occurring from solidification of saturates in vegetable oil, rapidly grow and causes filter plugging. [35] Because of the poor cold properties of vegetable oils, their blend in volume is restricted. [1, 33]

A possible solution hindering filter plugging is to decrease the content of paraffin which cause the poor cold properties. This could potentially be done by installing a dewaxing catalyst in the HDA reactor for selective isomerization of branched paraffin. [1, 6] However, this opportunity will not be covered in this master thesis.

2.5 Chemical kinetics

Chemical kinetics is often used in order to better understand at what rate chemical reactions and processes occur. The rate changes with time and represent how long it takes for a reactant to transform into new products. It can be measured on several different systems, including the decomposition of triglycerides. [36] By using Arrhenius equation, see Equation 2.1, the rate constant (k_i) is given, depending on a pre-exponential factor (A), the activation energy (E_a), temperature (T) and the universal gas constant (R).

$$k_i = Ae^{(\frac{-E_a}{RT})} \tag{2.1}$$

In a study made by Meier et al. a thermal cracking model of waste cooking oil is formed where four different pathways are defined based on the number of carbon atoms on the molecule chain. The study was performed without any addition of hydrogen gas. Meier et al. have divided the four groups into the starting product, waste cooking oil (WCO, $>$ C18), followed by heavy bio-oil (HBO, C12 - C18), light bio-oil (LBO, C4 - C11) and bio-gas (BGO, $<$ C4). [37] An overview of the groups and their rate constant pathways are shown in Figure 2.8.

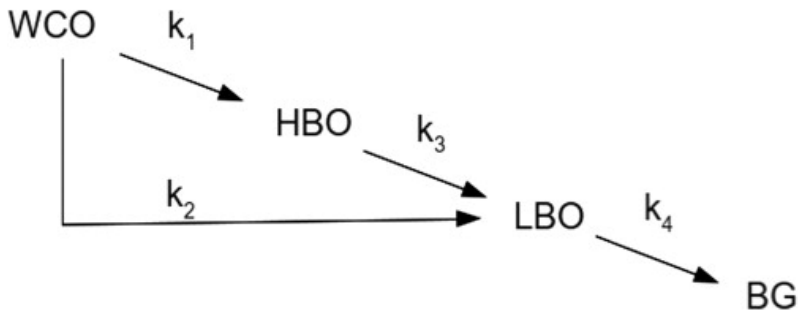

Figure 2.8: *Thermal cracking model.* [37].

The obtained rate constant from Arrhenius equation can be used in Equation 2.2 - 2.5 to determine the concentration of the different formed products and thereby determine the degradation of triglycerides at different times. [37]

$$C_{WCO}(t) = (C_{WCO})_0 e^{-(k_1+k_2)t} \tag{2.2}$$

$$C_{HBO}(t) = \alpha(C_{WCO})_0 e^{-(k_1+k_2)t} + [(C_{HBO})_0 - \alpha(C_{WCO})_0]e^{-k_3 t} \tag{2.3}$$

$$C_{LBO}(t) = \beta(C_{WCO})_0 e^{-(k_1+k_2)t} + \chi[(C_{HBO})_0 - \alpha(C_{WCO})_0]e^{-k_3 t} + [(C_{LBO})_0 + (\alpha\chi - \beta)(C_{WCO})_0 - \chi(C_{HBO})_0]e^{-k_4 t} \tag{2.4}$$

$$C_{BG}(t) = (C_{BG})_0 + \frac{k_4}{(k_1+k_2)}\beta(C_{WCO})_0[1 - e^{-(k_1+k_2)t}] + \epsilon[(C_{HBO})_0 - \alpha(C_{WCO})_0](1 - e^{-k_3 t}) \; [(C_{LBO})_0 + (\alpha\chi - \beta)(C_{WCO})_0 - \chi(C_{HBO})_0](1 - e^{-k_4 t}) \tag{2.5}$$

Where α, β, χ and ε are variables derived from Equation 2.6 - 2.9. [37]

$$\alpha = \frac{k_1}{k_3 - k_1 - k_2} \tag{2.6}$$

$$\beta = \frac{1}{k_4 - k_1 - k_2}[k_2 + \frac{k_1 k_2}{k_3 - k_1 - k_2}] \tag{2.7}$$

$$\chi = \frac{k_3}{k_4 - k_3} \tag{2.8}$$

$$\epsilon = \frac{k_4}{k_1 - k_3} \tag{2.9}$$

2.6 Corrosion

Corrosion is an electrochemical process occurring due to an oxidation-reduction reaction between a metal and its surrounding environment. In the reaction the metal acts as an anode being oxidized and releasing electrons to its surroundings. [38] For corrosion to occur a cell must be initiated. A cell is a circuit where electrons and ions are transported from one charged electrode to another. [39] Corrosion can generally be divided into two sections; internal- and external corrosion with internal corrosion being in focus in this master thesis. Internal corrosion, occurring in refinery pipelines, storage tanks *etc.*, are driven by contaminants in the petroleum feed such as sulfur and oxygen. [38]

The rate of corrosion for various types of materials can vary considerably in different environments. The reason for this is due to the energy levels of the materials and its

surroundings. A material strives to have as low energy level as possible. For produced materials such as steel, the energy level in the material will be high in comparison to the energy levels in nature. To decrease the energy levels of the material a process will start reacting and decomposing the produced steel back to its origins, *i.e.* corrosion occurs. A rule of thumb says, the more energy required to produce a material or alloy, the higher rate of corrosion the material will be exposed to. [39]

In this master thesis the main corrosion investigations will be laid on fatty acid corrosion, aqueous corrosion and ammonium salt corrosion.

2.6.1 Passivity

A protective thin film can be formed on the metal surface in corrosive environments. This film will reduce the corrosion rate of the metal providing a corrosion resistance even though it is not visible to the naked eye. The film is formed under oxidizing conditions together with a high anodic polarization. [40] To understand the formation of such a protective film, a polarization curve which represents the active-passive behavior of corrosion can be used. A general example of such a curve is shown in Figure 2.9.

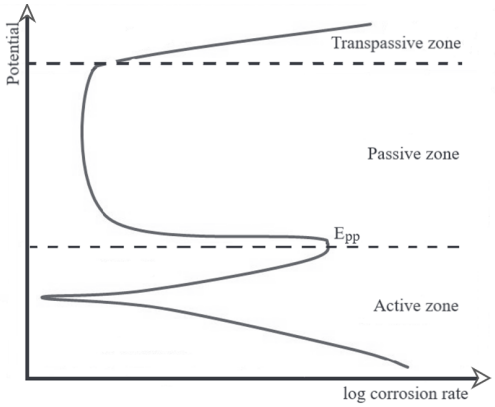

Figure 2.9: *An example of a polarization curve.*

The active zone has a low potential where the anodic current is high and increases within the zone. Above the passive potential (E_{pp}) the passive zone begins. In this zone the formed passive film becomes stable which reduces the corrosion rate significantly. It is therefore desirable for materials to stay in the passive zone. In the transpassive zone the passive film starts to break down, increasing the corrosion rate. [40]

In Figure 2.10 Pourbaix diagrams for iron and chromium are shown. [41] These figures present the possible types of stable protective films at varying potential and pH. As can be seen in the figures, the formed protective films on iron are usually of oxides, Fe^{2+} and Fe^{3+} whereas for chromium the film consists of oxides, Cr^{2+} and Cr^{3+}.

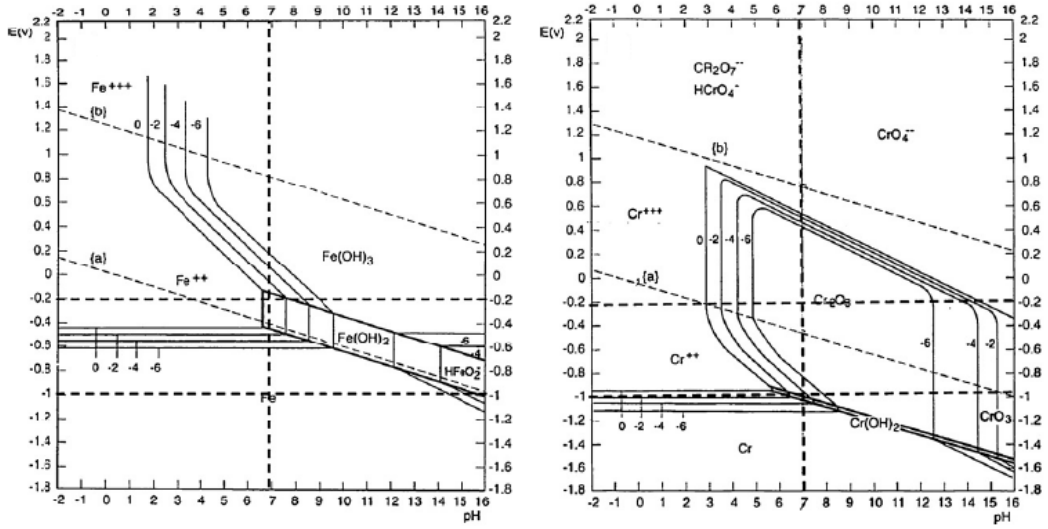

Figure 2.10: *Pourbaix diagram for iron and chromium.* [41]

When comparing the oxide formation between iron and chromium one can observe that a stable formation of Cr_2O_3 is formed at significantly lower potential then for Fe_3O_4. This makes the element of chromium desirable when designing feed pipes and other equipment in corrosive environments such as the oil and gas industry. However, the thin protective films can break down causing localized corrosion due to its fragility. [40]

2.6.2 Fatty acid corrosion

With fatty acids being the main component in triglycerides, exposing the steel of the inlet pipe to the HDS reactor, this is one of the main interests in this master thesis. They are complicated from a corrosive point of view since organic acids often is included in a process mixture together with other organic acids, salts or inorganic acids. [20]

In a comparison between tall oil, which is used as a renewable source of feed in Preems refinery in Gothenburg, and vegetable oils, the later show less risk of corrosion. This is due to the characterization of steric and palmitic acids in vegetable oils. Previous published investigations have showed that alloy 316L have had a fulfilling corrosion resistance in this type of feed. [20]

2.6.3 Ammonium salt corrosion

The gaseous stream from the interstage stripper and HDA reactor, including components of H_2S, NH_3 and HCl, can react into acid salts. Two common types are ammonium chloride (NH_4Cl) and ammonium bisulfide (NH_4HS). The formation of these salts is presented in Equation 2.10 - 2.11. [42] Before the revamp of the SynSat unit, chlorides was estimated to < 1 ppm, whereas the rapeseed oil contains > 12 ppm chlorides. This can cause a salt deposition of NH_4Cl to occur at temperatures where no deposition of NH_4Cl occurred

before the revamp according to diagrams. [9] This new increased amount of chlorides makes the ammonium salt corrosion of interest when investigating the effects of adding rapeseed oil into a revamped SynSat unit.

$$NH_3 + HCl \rightarrow NH_4Cl \tag{2.10}$$

$$NH_3 + H_2S \rightarrow NH_4HS \tag{2.11}$$

As shown in Equation 2.10, ammonium chloride is the product of ammonia and hydrogen chloride and is corrosive in both gas, solid or in solution and comes in the form of both general and local corrosion. [43] The deposition of ammonium chloride occurs from the vapor phase where ammonia and hydrogen chloride are present. This occurs when the stability constant of ammonium chloride is smaller than the molar partial pressures of ammonia and hydrogen chloride. The deposition of the salt firstly comes in the forms of small molecules in vapor phase which with time increases into larger particles. [44] The absence or limited amount of water in a system where ammonium chloride is present causes the propagation of pitting corrosion, which can be read about in Section 2.6.4.1. [43]

Ammonium bisulfide, the product of ammonia and hydrogen sulfide presented in Equation 2.11, can also be found in the upstream of the interstage stripper and HDA reactor in the revamped SynSat unit. As for ammonium chloride, the propagation for deposition of ammonium bisulfide can occur when smaller amounts of water is present. The deposition of the salt can cause fouling in heat exchangers or/and air cooler pipes. [45]

2.6.4 Aqueous phase corrosion

Carbon dioxide and hydrogen sulfide are the two acid gases which have the greatest impact on the corrosion rate of a system. [46] After the revamp of the SynSat unit, some of the triglycerides in rapeseed oil will react in unwanted HDC reactions giving products of carbon dioxide and carbon monoxide as seen in Section 2.3.1. It is the increased amount of these substances that will be investigated further together with the already present hydrogen sulfide. Noticeable is the decreased amount of hydrogen sulfide when co-processing rapeseed oil with fossil feed due to less amount of sulfur in the total feed.

Different phases, such as gas, liquid hydrocarbons, gas condensate and liquid water phase, can be present in the SynSat unit, singly or in a combination with other phases. The phases changes depending on its location in the unit, for example being liquid hydrocarbons into the HDS reactor and then gaseous in the amine absorber. These changes of phases can affect the rate of corrosion in the system. [46] In the upstream system of the interstage stripper and HDA reactor, there are streams with phases of mixed liquid/vapor and streams with only vapor phase.

The gas phase from the interstage stripper and the HDA reactor is a combination of mainly hydrocarbons and acid gases where the acid gases are of main interest with respect

to corrosion. The liquid water phase formed can be produced water, injected and/or condensed water. This occurs when the temperature and pressure changes and entails in acid gases of carbon dioxide and hydrogen sulfide in the water. The liquid water is of great importance when it comes to corrosion in pipes since the liquid stays in contact with the pipe material. [47] In the SynSat unit before the revamp, a water injection point is set between the HHPS and the HHPS vapor effluent cooler in the upstream feed of the interstage stripper and HDA reactor. This is done to avoid fouling and corrosion of tubes due to build-up of salts crystals like ammonium chloride and ammonium bisulfide. The addition of water can initiate reactions between the acid gases of carbon dioxide and hydrogen sulfide and the pipe steel material which may cause internal corrosion. The chemical corrosion reactions of this can be seen in Section 2.6.5.

Corrosion occurring from carbon dioxide in a hydrogen sulfide free environment is usually named *sweet* corrosion and is defined by the dissolved carbon dioxide gas in water phase. Environments containing hydrogen sulfide is called *sour* corrosion. Unlike sweet corrosion, sour corrosion can contain both hydrogen sulfide and carbon dioxide. [46] In order to predict whether sweet or sour corrosion is formed, the type of corrosion product must be identified, see Table 2.3. Studies indicate that for carbon steel, a CO_2/H_2S ratio < 20 gives sour corrosion, a CO_2/H_2S ratio between 20 - 500 gives a mixed regime of sour and sweet corrosion product whereas sweet corrosion is formed at a CO_2/H_2S ratio > 500. [48]

Table 2.3: *Dominating corrosion forms in carbon steel at different partial pressure ratios of CO_2 and H_2S.* [48]

ppCO$_2$/ppH$_2$S ratio	**Dominating corrosion form**
< 20	H_2S corrosion
20 - 500	Mixed CO_2/H_2S corrosion
> 500	CO_2 corrosion

Calculations of a CO_2/H_2S ratio is a commonly used method by the gas and oil industry in order to determine whether a system is of sour, mixed or sweet dominance. Originally the influence of temperature on the ratio was not investigated but set to 25 °C. [49] This temperature is far below the temperatures which can be used in the gas and oil industry including the SynSat unit. Later on the temperature acceptance has been increased to a range between 25 - 100 °C since the impact the thermodynamic data was still minor at this point. At higher temperatures > 100 °C changes of protective films starts to arise. [49]

In Figure 2.11 the relationship between different possible corrosion product on carbon steel is shown. When calculating the ratio of sour or sweet corrosion some assumptions are taken which will be presented below. The first assumption is the presence of both mackinawite, one type of iron sulfide, and iron carbide. Therefore the line between these corrosion products is the valid line for the ratio calculations. At temperatures below this line the the equilibrium is instead between iron ions (Fe^{2+}) and mackinawite which are not

valid for the ratio calculations. At temperatures above the equilibrium of iron carbide and mackinawite the equilibrium instead lies between iron carbide and pyrrhotite or troilite. This is not a valid line for the ratio calculations either since these assume mackinawite to be the produced iron sulfide corrosion product. Pyrrhotite and troilite are both more stable compounds then mackinawite and the ratio for sweet corrosion should therefore be converted from 500 to at least 2500. [49]

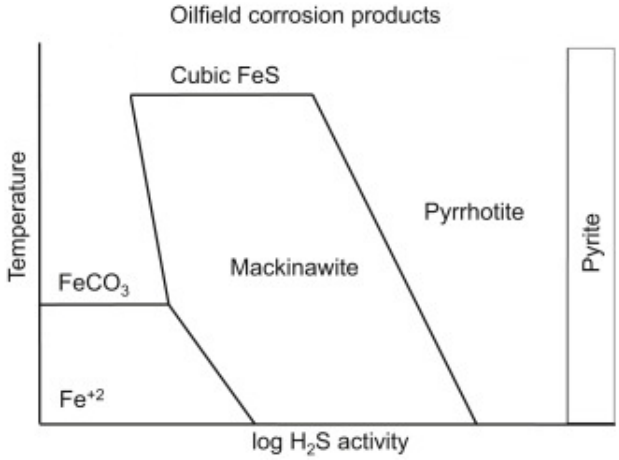

Figure 2.11: *Relationships of corrosion products on carbon steel.* [47]

2.6.4.1 Sweet corrosion

Corrosion occurring due to carbon dioxide has been a recognized problem in the oil and gas industry for many years. Carbon dioxide itself does not cause corrosion but with the presence of water, corrosion products of iron carbonate ($FeCO_3$) is formed according to Equation 2.12. [11, 50]

$$Fe + CO_2 + H_2O \rightarrow FeCO_3 + H_2 \tag{2.12}$$

Iron carbonate normally forms a protective film layer on the metal surface which can reduce the reaction rate. The reduction of reaction rate is due to that the reactants have to diffuse through the protective $FeCO_3$ layer. At higher temperatures (>100 °C) iron oxide (Fe_3O_4), also called magnetite, can be formed as a corrosion product. [51] It is however possible for the protective film layer to break down due to different stresses or high feed velocity. If this occurs areas where the protective film has broken down may be exposed to local corrosion. [50]

During sweet corrosion, several different types of corrosion can occur on the steel surface, for example uniform and pitting corrosion. [11] Uniform corrosion is characterized by corroded areas over most or all of the material. The depth of corrosion can vary, but

does not include any small local peaks of corrosion. [52] In uniform corrosion the water present in the feed can condense and adsorb on the pipe walls, creating a film of water. This occurs when the carbon dioxide being present in the system dissolves in water. [11] Uniform corrosion is the most common type of corrosion and the least dangerous. [53]

Another characteristic type of corrosion in sweet environments is pitting corrosion. [11] In the opposite to uniform corrosion, pitting corrosion is characterized by taking place in local zones. The rates of corrosion are often high, with several orders greater than for uniform corrosion. [52] Pitting corrosion occurs due to failed or uneven protective films of iron carbide or iron oxide in local areas, causing small peaks. [11]

2.6.4.2 Sour corrosion

The definition of sour corrosion can be determined by the presence of hydrogen sulfide, forming protective corrosion layers of iron sulfides. [47] As for carbon dioxide, hydrogen sulfide itself is rather harmless from a corrosive point of view. However, in contact with water it easily dissolves and may form the corrosion product of iron sulfide according to Equation 2.13. [11]

$$Fe + H_2S \rightarrow FeS + 2H \tag{2.13}$$

At temperatures below 100 °C, mackinawite is the main formed hydrogen sulfide corrosion product. This is due to the fact that mackinawite has a faster kinetics then other hydrogen sulfide corrosion products such as pyrrhotite at the elevated temperatures. [47, 51] The formation of mackinawite occurs on the steel surface when iron sulfide is still soluble in the bulk. This occurs when the concentrations of Fe^{2+} and hydrogen sulfide lays below the saturation level. At temperatures above 100 °C the concentration of iron sulfide meets or exceed the saturation levels, pyrrhotite is the main formed product. [47] It is however believed that mackinawite is initially formed product, which later decomposes to pyrrhotite. [54]

In sour corrosion environments many types of corrosion can occur, with two of the most common of them being hydrogen-induced cracking (HIC) and stress corrosion cracking (SSC). [11, 50] In HIC the presence of hydrogen atoms in the metal causes the material to gain a tensile stress. This occurs when the hydrogen atoms diffuse through the metal, reacting into hydrogen molecules which are insoluble in steel. The effect of the gained tensile stress initiates HIC. SCC occurs due to the breakdown of the protective oxide film on the metal surface. Without any film, sulfide particles can more easily react with the steel surface, allowing it to corrode. The cracking occurs due to localized hydrogen embrittlement in the steel. [55]

2.6.5 Corrosion reactions

The chemical reactions due to the presence of naphthenic acids is presented in Equation 2.14 - 2.15. In the first reaction iron atoms on the metal surface is attacked by naph-

thenic acids forming a product of iron naphthenates and hydrogen gas. In the second reaction hydrogen sulfide corrosion can occur when the formed iron naphthenates reacts with hydrogen sulfide, forming more naphthenic acids and hydrogen gas while also inhibiting soluble iron to be produced. Depending on the amount of sulfide compounds present in the reactions the production of iron sulfide and corrosion varies. Formed iron naphthenates is a product of corrosion whereas iron sulfide forms a protective film on the metal surface. [53]

$$Fe + 2RCOOH \rightarrow Fe(RCOO)_2 + H_2 \tag{2.14}$$

$$Fe(RCOO)_2 + H_2S \rightarrow FeS + 2RCOOH \tag{2.15}$$

The corrosion mechanism of the steel material for both sweet and sour corrosion is an anode reaction where the solid iron reacts into an iron (Fe^{2+}) ion according to Equation 2.16. [11]

$$Fe \rightarrow Fe^{2+} + 2e^- \tag{2.16}$$

The main reactions of sweet corrosion and the formation of a protective oxide layer is presented in Equation 2.17 - 2.20. In the initial reaction carbon dioxide reacts with the injected water forming carbonic acid (H_2CO_3) which later reacts into the more corrosive substance of bicarbonate (HCO_3^-) ions. The bicarbonate then, together with an electron, forms carbonate (CO_3^{2-}) ions which in the final reaction creates the protective oxide layer of $FeCO_3$. [11, 51]

$$CO_2 + H_2O \rightarrow H_2CO_3 \tag{2.17}$$

$$H_2CO_3 + e^- \rightarrow HCO_3^- + 0.5H_2 \tag{2.18}$$

$$HCO_3^- + e^- \rightarrow CO_3^{2-} + 0.5H_2 \tag{2.19}$$

$$Fe^{2+} + CO_3^{2-} \rightarrow FeCO_3 \tag{2.20}$$

The corresponding reaction mechanisms for sour corrosion is presented in Equation 2.21 - 2.23. Initially hydrogen sulfide dissolves in water rather easily depending on the partial pressure and temperature of the system. The H_2S being dissolved may then quickly be ionized giving sulfur (S^{2-}) ions and hydrogen ions. Due to a strong depolarization of the hydrogen ion, electrons from the steel forms hydrogen ions into hydrogen atoms. The iron in the steel then reacts with the formed S^{2-} ions producing a protective film of FeS. [11]

$$H_2S \rightarrow HS^- + H^+ \tag{2.21}$$

$$HS^- \rightarrow S^{2-} + H^+ \tag{2.22}$$

$$Fe^{2+} + S^{2-} \rightarrow FeS \tag{2.23}$$

2.6.6 Corrosion prediction of H_2S and CO_2

Published studies indicates that the formed layers of corrosion products can be of great importance when it comes to reducing the corrosion rates. [56] For example, the type of formed iron sulfide in a sour corrosive environment will affect the hydrogen absorption to a material and hence affect its risk of hydrogen induced damage. [57] The formed corrosion product could force sulfide or carbide particles to diffuse through the film layer before reacting with the steel material. [56]

Several corrosion prediction models for carbon dioxide environments have been established during the years. However, for hydrogen sulfide or mixed carbon dioxide/hydrogen sulfide corrosion it has been found to be more difficult to predict since the corrosion mechanisms are more uncertain. [56, 58] Studies have indicated that with hydrogen sulfide present in the system many different types of iron sulfides can form on the steel material. Mackinawite is the first film layer formed as a product of the mixed carbon dioxide/hydrogen sulfide or hydrogen sulfide environment. The initial formation occurs quickly on the steel forming a solid inner mackinawite layer by a solid-state reaction (see Equation 2.13). This layer ($\ll$ 1 µm) is a tight film layer which act as a barrier, forcing the sulfide particles to diffuse through the layer before reaching and reacting with the steel. Outside of the inner layer a larger porous film ($\gg$ 1 µm) is formed also working as a diffusion layer for the sulfide particles. It is believed that the corrosion process for hydrogen sulfide also is valid for a mixed carbon dioxide/hydrogen sulfide corrosion, along with smaller adjustments. [56]

2.6.7 Total acid number

To measure the corrosivity of the types of corrosion described in this section one can use the Total Acid Number (TAN). TAN is a measurement of acidity in a liquid and is determined by the amount of KOH needed in order to neutralize 1 gram of sample [3, 59]. The measurements represent a value for the overall acidic components in the crude oil. [53] TAN also measures the degree of oxidation and hydrolysis in the sample of renewable diesel. With a high degree of either oxidation or hydrolysis, formation of free fatty acids can occur. It is the free fatty acids that can cause the main corrosion problems in pipe or equipment. [3]

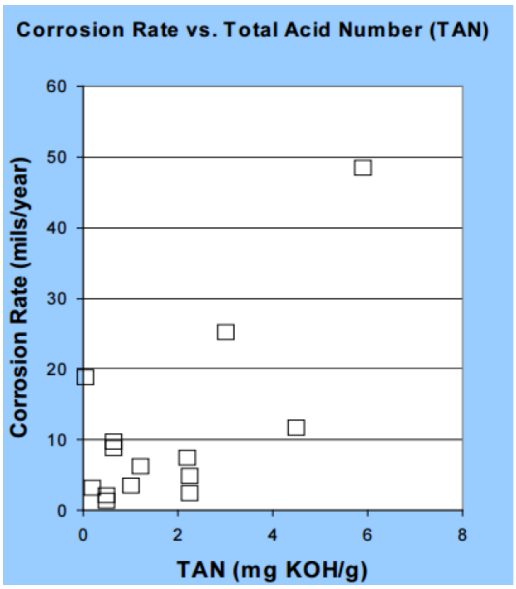

Figure 2.12: *Correlation between corrosion rate and TAN for several crude oils.* [13]

Crude oils refined today usually have a TAN value between 0.05 - 6.0 mg KOH/g and can be divided into high acid crude and acid crude. [60] High acid crudes are represented by naphthenic acids and have a TAN value $>$ 1.0 mg KOH/g whereas acid crudes are acids which have a TAN value $>$ 0.5 mg KOH/g. [61] Crude oils with $<$ 0.5 mg KOH/g are seen as rather harmless from a corrosion point of view at Preem. It is however important to know that there are several aspects deciding the corrosivity of a feed, such as the process temperature, feed rate, amount of sulfur, acid structure *etc.* [53, 50] Measuring TAN only yields a rough estimate of the corrosiveness of the sample since crude oils with similar TAN values can differ in corrosivity as shown in Figure 2.12. [53]

The current TAN value in the SynSat unit varies with which type of crude oil being refined. High sulfur (HS) and low sulfur (LS) provides different characteristics to the LAGO which is important to take in consideration when evaluating the measured TAN results.

Many studies have been made, trying to identify the acid compounds in different crude oils, including using nuclear magnetic resonance (NMR), gas chromatography (GC), high performance liquid chromatography (HPLC) *etc.* No technique has however, been fully successful. The difficulty of identifying crude oil corrosiveness is that the position of the carboxylic acid group on the molecule does have a great impact on the reactivity of the acid. [13]

2.7 Steel materials

There are many types of materials used in Preem's refinery plant i Lysekil. One of them being stainless steel which will be further explained in the following section. Stainless

steel material of alloy 321 is the current material at the inlet of the HDS reactor whereas the materials used at the upstream feed of the interstage stripper and HDA reactor varies. Which type of material is however confidential and will therefore not be further discussed.

The material and its alloy composition has a vital effect for corrosion resistance of a system. Molybdenum, for example, enhances the formation of the protective corrosion film layer. It can also capture diffused hydrogen by formation of carbides. Capturing hydrogen can in turn reduce the risk of hydrogen induced corrosion. [57]

2.7.1 Stainless steel

The inlet pipe to the HDS reactor is today made of alloy 321, a titanium stabilized austenitic stainless steel. [62] Alloy 321 is planned to be the material used in the inlet pipeline as well after the revamp of the SynSat unit. It is however unknown how this material will resist fatty acid corrosion attacks during co-processing of rapeseed oil in the revamped SynSat unit.

Materials of stainless steel are used favorably in sulfur environments above 290 °C, due to its added element of molybdenum. [25] With an increase in operating temperature in the process unit, an increase of molybdenum content is required. [20] There are over 100 different grades of stainless steel materials available on the market today and they all are defined by a composition with iron $> 50\%$ and chromium of at least 10 - 12%. [63, 64] Often other elements are included, like a low content of carbon, but it is not needed for the requirement to be named stainless steel. The material can be classified into five different subgroups with austenitic stainless steel (ASS) being of specific interest in this master thesis. [63]

Austenitic stainless steel is usually recognized by its high amount of chromium and nickel content, whereas the carbon is usually held at low content since it is considered an unwanted impurity. [65] The addition of nickel stabilizes the face center cubic phase and improves the resistance of corrosion on the material. [40] This group does show excellent mechanical properties, including toughness and strength. [66] ASS has the highest corrosion resistance of all subgroups and is commonly used for several applications. [64]

In general, chromium together with a low carbon content will yield stainless steel material with great resistance to both corrosive environments and heat. [64, 67] Chromium is also the most important element for formation of thin protective films on the metal surface. [40] It is however the addition of nickel that makes the stainless steel a functional and adaptable material. In comparison with other non-nickel stainless steel, nickel containing alloys is non-magnetic and will remain ductile at low temperatures but still being able to use for applications at high temperatures. These features make the nickel content in stainless steel of great importance since it enables usage of many different applications. [67] Elements as titanium or columbium are commonly added to the stainless steel in order to reduce the corrosion by converting the carbon content into stable carbide. The carbon content in the alloy can alternatively be $< 0.03\%$ and thereby avoid intergranular corrosion. [20] Other elements such as molybdenum could be added in order to increase the

corrosion resistance further in variable environments. [64] In specific, molybdenum gives an increased resistance to naphthenic acid corrosion in crude units since molybdenum stabilizes the protective passive film from different types of organic attacks commonly in refinery units. [68]

When designing and choosing materials for the inlet pipe at the revamped SynSat unit the main objective is corrosion resistance. Austenitic alloys with a combination of chromium, molybdenum, nickel and nitrogen are commonly chosen for this type of application. This classification of austenitic alloys includes 316 and 317L, which will be described further in the Section 2.7.1.1. [65]

2.7.1.1 Comparison of austenitic stainless steel materials

The titanium stabilized alloy 321 is of austenitic stainless steel classification with an excellent corrosion resistance up to about 820 °C. [62] Alloy 321 does have a high chromium (18%) and nickel (11.5%) content together with a smaller content of other elements such as manganese and carbon. [62] As seen in Table 2.4, only alloy 321 does have a content of titanium. The titanium avoids precipitation of the material by converting carbon into stable carbide. [20]

Stainless steel alloy 316 is based on a chromium, nickel and molybdenum content and is commonly used in chemical and petrochemical processes as vessels, tanks and pipe lines. [69] The last alloy of comparison is alloy 317L, an austenitic stainless steel of chromium, nickel and molybdenum as the main elements. The combination and high level of these main elements provides the alloy with a better corrosion resistance in comparison to the more traditional alloys of types 304 and 316. [70]

Table 2.4: *Chemical analysis of ASS alloy 321, 316 and 317L in wt%.* [62, 69, 70]

Element	**alloy 321**	**alloy 316**	**alloy 317L**
Cr	17.00 - 19.00	16.00 - 18.00	18.00 – 20.00
Ni	9.00 - 12.00	10.00 - 14.00	11.00 – 15.00
C	0.08	0.08	0.03
Mn	2.00	2.00	2.00
P	0.045	0.045	0.045
S	0.030	0.03	0.030
Si	0.75	0.75	0.75
Ti	0.70	-	-
N	0.10	0.1	0.10
Mo	-	2.00 - 3.00	3.00 – 4.00
Fe	Balance	Balance	Balance

3 Methodology

In this section literature methods, apparatus and analytical methods used during the project are described. A literature study was performed on several topics, focusing on the current and revamped SynSat process and what the changes will result in from a process and material point of view. Chemical structure of triglycerides and compounds such as hydrogen sulfide and carbon dioxide were also investigated. In addition to published articles, different types of corrosion and of corrosion prediction models were included in the literature studies. The methodology also included literature studies of different types of stainless steels and what a difference in content can make between different type of materials. The main source of information during this project have been read through published studies found mainly from publications of *Fuel Processing Technology, Materials Science and Engineering, Fuel etc.* and published books of material science.

3.1 Heat treatment of co-processed feed

To investigate the potential risks of corrosion when rapeseed oil and LAGO are being co-processed before entering the HDS-reactor, such a simulation must be created. In this master thesis this simulation was performed in a co-operation with Research Institutes of Sweden (RISE). RISE is a Swedish state owed company which collaborate on behalf of private and public sectors together with Swedish universities. [71]

At one of RISE laboratories in Södertälje, Sweden, four different mixtures of rapeseed oil (5, 10, 15 and 100 wt%) were mixed with a balanced amount of LAGO. All four samples was then heated to temperatures of 290, 310 and 330 °C in a hydrogen gas environment in order to simulate the process before the HDS reactor, seen in Figure 2.3. In Table 3.1 the different samples tested at RISE are lined up.

3.1.1 Heat treatment execution

To simulate the continuous plug flow reactor, a ½" column made out of stainless steel 316L material was prepared with glass wool in its bottom end in order to avoid larger particles to be able to flow further after the column. The column had a wall thickness of 0.89 mm and the length of 827 mm, giving a reactor volume of 77.5 ml. Thereafter the whole column was filled with 125.6 g of silicon carbide (coarse, 46 grit) with purpose to give an even heat transfer of the flow. The column was then mounted and installed by adding a thick protective steel layer outside of the column in order to have an even

Table 3.1: *Samples tested for simulation of co-processing feed at RISE.*

Sample	Temperature [°C]	Rapeseed oil [wt%]	LAGO [wt%]
1	290	5	95
2	290	10	90
3	290	15	85
4	290	100	0
5	310	5	95
6	310	10	90
7	310	15	85
8	310	100	0
9	330	5	95
10	330	10	90
11	330	15	85
12	330	100	0

temperature of the outside column. Outside of the protective layer, an oven was placed, see Figure 3.1 The suppliers of LAGO and hydrogen gas were installed into a joint pipe that was connected to the head of the column whereas the pipe supplying rapeseed oil was added in another injection point to the head of the column. The two liquids were assumed to be completely mixed after this point.

Thereafter the whole apparatus was cleaned thoroughly part by part with acetone in order to ensure that all residues of old samples was cleaned out of the system. With old samples still left in the system the later measurements of TAN can be greatly affected. After cleaning the apparatus system with acetone, it was run with rapeseed oil in order to dilute any traces of the acetone. A pressure test was then performed on the system with nitrogen gas at 48 bar in order to ensure that there was no leak in the system.

With a total column volume of 77.5 ml and a LHSV set to 1.5 a total flow of 1.94 ml/min was run through the reactor. In Table 3.2 the different volumes of LAGO and rapeseed oil for the different samples are presented.

Table 3.2: *Flow of rapeseed oil and light gasoil for the different samples.*

	Rapeseed oil [ml/min]	Light gasoil [ml/min]
Sample 1, 5 and 9	0.0975	1.8425
Sample 2, 6 and 10	0.1950	1.745
Sample 3, 7 and 11	0.2925	1.6475
Sample 4, 8 and 12	1.940	-

The tests were performed with constant temperatures, while only the wt% of rapeseed oil was changed. After the three different blends (5, 10 and 15 wt%) were tested isothermally, the temperature was increased, and the experiments repeated. Samples with 100

wt% was performed lastly as to avoid possible coke on the silicon carbide in the column. Performance of each test took three hours. Two hours was set to ensure steady state and thereafter 90 ml of sample was collected. For further explanation of steady state and time schedule during the test see Figure A.1 in Appendix 1. All 12 samples were performed with the same approach.

3.1.2 Equipment

In Figure 3.1 a simplified image of the laboratory set-up at RISE is shown. Green lines represent liquid in the form of rapeseed oil or LAGO whereas red lines represent nitrogen and hydrogen gas. The black lines post the fixed bed column represent the two completely mixed components.

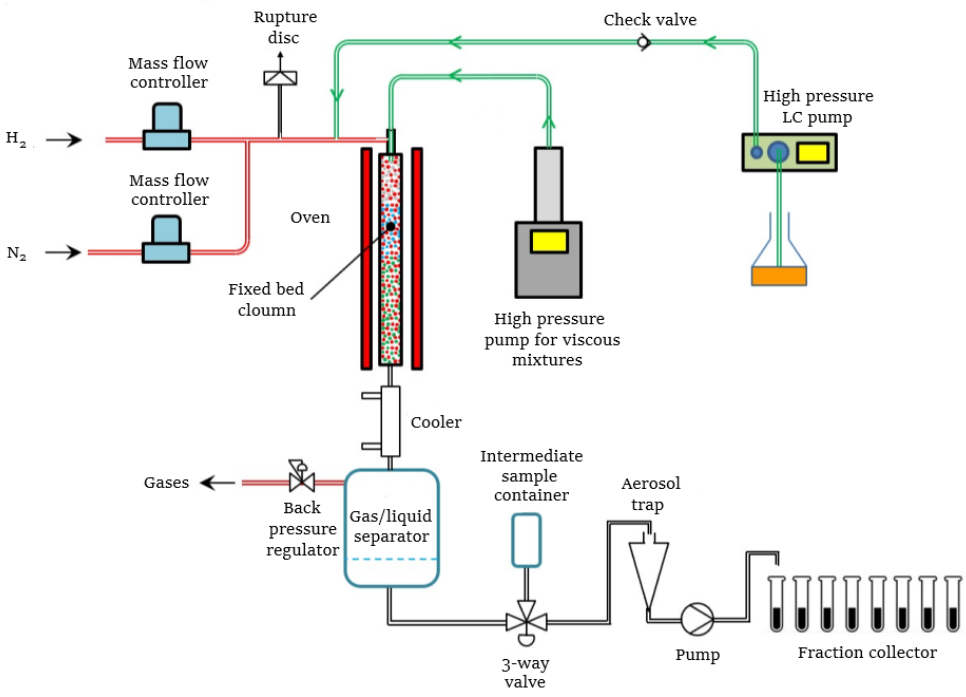

Figure 3.1: *The equipment set-up for heat treating of LAGO together with hydrogen gas and rapeseed oil. Provided and approved by Research Institutes of Sweden.*

A high pressure LC pump is pumping the LAGO towards a check valve and further on towards the oven where it will mix with the hydrogen gas. In the high pressure pump for rapeseed oil, a moving piston will compress the liquid. Two check valves with opposing directions will result in a vacuum which forces the rapeseed oil to enter the cylinder. At the other check valve, the liquid will be pumped towards the process. Rapeseed oil will then flow through small pipes to the head of the column where the feed will meet with the hydrogen gas mixed light gasoil. The blended feed will then pass through the fixed bed column, fully filled with silicon carbide. Around the column a thicker shell is attached

to give an even temperature for the whole column. Outside of the shell an oven will heat the column to desired temperatures of 290, 310 and 330 °C. At three different points small temperature measurements are attached. These measurements verify a homogeneous temperature over the whole column.

When the heated feed has passed through the column, a cooler will reduce the temperature of the feed before it enters a gas/liquid separator. In the gas/liquid separator the liquid is settled on the bottom of the cylinder whereas gas stays at the top of the cylinder and can be removed from the separator via a back pressure regulator. The intermediate sample container receives 30 ml liquid from the liquid/gas separator every 15 minutes. This in order to avoid the gas/liquid separator to be over filled with feed from the column. From the intermediate sample container, the liquid flows towards an aerosol trap, where it will come out as a mixture of liquid and foam due to the high pressure in the system. The liquid is then pumped towards a waste container before steady state is reached and thereafter to the sample container.

3.2 Analysis of acid number

Measurements of total acid number performed in this master thesis is based on standard ASTM D664 [72] with some modifications. In the original method KOH of 0.1 M is used whereas Preem's laboratory in Gothenburg uses 0.01 M KOH. By using weaker concentrations of KOH, less amounts of sample are needed than in the original method and the sample will more easily dissolve in the titration solution.

Measurements were performed on all samples listed in Table 3.1 above together with an addition of three samples shown in Table 3.3. The three samples were not heat treated, but are reference samples for mixtures of 5, 10 and 15 wt% rapeseed oil.

Table 3.3: *Reference samples tested.*

Sample	Rapeseed oil [wt%]	LAGO [wt%]
13	5	95
14	10	90
15	15	85

3.2.1 Analysis principle

The sample is dissolved in a titration solution and is titrated potentiometrically with alcoholic KOH (0.01 M) together with a combination electrode. The titration curve is continuously recorded, and the inflections are used as the end point for the titration. From the obtained curve, the voltage in relation to the added volume of KOH is seen and translated into mg KOH/g. Equivalence points are the part of the curve where the tangent line has the steepest slope and is where the acids react.

A specified endpoint, called the fixed point, is used as a reference point when measuring the total acid number. This point represents the amount of alkali (mg KOH/g) needed to neutralize the sample to a specific endpoint which corresponds to pH 10. Depending on

the electrode different values are obtained; during these tests the electrode is calibrated to -134.3 mV.

3.2.2 Analysis execution

Firstly, a solution of KOH (0.01 M) was prepared by pipetting 50 ml of 0.1 M KOH in isopropanol (IPA) into a 500 ml volumetric flask. The solution was then diluted by IPA to a total of 500 ml. The solution was then added to a flask and installed to the TAN measurement system. Lastly 40 ml of the newly mixed KOH (0.01 M) was run through the system.

For TAN analysis, 5 - 10 g of sample was weighed and mixed together with 120 ml of titration solution (0.6 ml distilled water, 59.4 ml IPA and 60 ml toluene). The beaker was put on a magnet stirrer and an electrode together with a plastic pipe for addition of KOH (0.01 M) was submerged into the solution. After being stirred for 90 seconds in order to get a well-mixed solution, the test started.

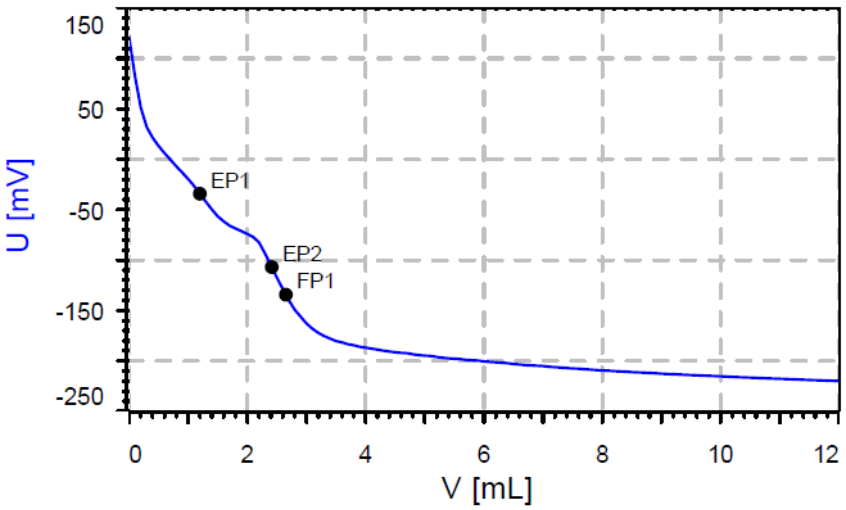

Figure 3.2: *Example of graph formed from TAN analysis.*

During the test KOH will be added continuously while the electrode will notice any reactions of acids. Meanwhile a graph of voltage (mV) plotted against added KOH volume (ml) is created. This graph is shown in Figure 3.2 where the two endpoints (EP) and the fixed point (FP) can be seen. When observing the two endpoints, it is desirable that it lies ± 25 mV from the fixed point. In the example showed in Figure 3.2 one can observe that EP2 is such a point whereas EP1 lies far away from the FP. Therefore, in this case, EP1 is what is called a ghost point and should not be taken in consideration. Another aspect is the desire to get the endpoints between the range of 2 - 8 ml of added KOH in order to get the highest resolution of TAN.

A Tiamo software then calculated the measured voltage and added volume of KOH into TAN (mg KOH/g) by Equation 3.1.

$$TAN = \frac{(A - B) * M * 56.11}{W} \tag{3.1}$$

where A equals ml KOH-solution added to the sample and B ml of KOH solution added to the blank. M stands for molarity of the KOH solution and W represent the weight (g) of the sample.

3.3 Chemical kinetics

The chemical kinetics of triglycerides are of great importance in order to better understand the risk of corrosion when co-processing rapeseed oil into the revamped SynSat unit. It was therefore investigated how much and at what rate the triglycerides are degrading and what effect the hydrogen gas has on this system.

To determine degradation of triglycerides in rapeseed oil at various times, Arrhenius equation (Equation 2.1) was used to calculate the reaction rates. A total of four reaction rates were calculated with help of known activation parameters (E_a) and pre-exponential factors (A) according to the study performed by Meier et al. The three investigated temperatures of 290, 310 and 330 °C was used in order to achieve three different rate constants for each product depending on the processing temperature. The calculated reaction rates (k_1 - k_4) for each temperature was then used in Equation 2.2 - 2.5 in order to determine the concentration of the four products at selected times. All calculations were based on the kinetic model presented by Meier et al. [37]

3.4 Ammonium salt corrosion

Ammonium chloride and ammonium bisulfide both easily dissolve in water. [73] Therefore an injection point of wash water dissolving the salts is a common solution to avoid corrosion and fouling due to ammonium salts. It is however important to understand where this injection point of wash water should be installed to reduce the risk of ammonium salt corrosion. In order to do this it is of great importance to know if deposition of salt occurs in the the feed pipes and where.

Calculations were performed on the different streams of A, B, C, E and F, seen in Figure 2.5 in Section 2.2.1, in order to predict where the wash water streams are necessary to avoid ammonium salt deposition. The calculations were based on the stream temperature for each stream and salt stability constant of the two ammonium salts, K_{NH_4Cl} and K_{NH_4HS} where the stability constant for ammonium chloride is the partial pressure of ammonia and hydrogen chloride according to Equation 3.2. [43]

$$K_{NH_4Cl} = p_{NH_3} * p_{HCl} \tag{3.2}$$

The stability constant for hydrogen bisulfide is the partial pressure of ammonia and hydrogen sulfide according to Equation 3.3. [43]

$$K_{NH_4HS} = p_{NH_3} * p_{H_2S}. \tag{3.3}$$

The salt stability constant for ammonium chloride and ammonium bisulfide is, as seen above, based on the partial pressures for HCl, NH_3 and H_2S. These partial pressure values were calculated from Equation 3.4 - 3.6.

$$p_{HCl} = (P + 1.013) * 14.5 * N_{HCl} \tag{3.4}$$

$$p_{NH_3} = (P + 1.013) * 14.5 * N_{NH_3} \tag{3.5}$$

$$p_{H_2S} = (P + 1.013) * 14.5 * N_{H_2S} \tag{3.6}$$

Where P represent the total stream pressure in bar and N represent the mole fraction for each compound. The addition of 1 atm in the equations can be related to the pressures being stated in over pressure (bar) whereas the diagram presented in Appendix II as Figure A.2 and A.3 uses absolute pressure (psia). Therefore a uniform pressure unit is desirable for the later calculations.

By calculating the stability constants values in Equation 3.2 and 3.3 and knowing the accurate temperature of each stream the occurrence of deposition of ammonium salts could be decided from diagrams presented in Figure A.2 - A.3 in Appendix II. [9, 74]

3.5 Corrosion prediction of H_2S and CO_2

In order to determine whether or not there is a significant risk of sour or sweet corrosion in the upstream system of the interstage stripper and the HDA reactor the phase for each stream A, B, E and F has to be calculated. The partial pressure for water can be calculated by an extension of Dalton's law according to Equation 3.7. Where p_{tot} and n_{tot} represent the pressure and substance amount for the total stream and x represent the investigated compound.

$$p_x = p_{tot} * (\frac{n_x}{n_{tot}}) \tag{3.7}$$

Calculating the water partial pressure for the amine recovery system of the SynSat unit one assumption had to be done. The data for p_{tot} and n_{tot} had to be assumed to be all in vapor phase which is not completely true. The actual vapor fractions will be presented in Section 4.6 together with the calculated partial pressure results. From the calculated partial pressure values of water a steam pressure curve by Mörtstedt and Hellsten was used to predict at which temperature the water evaporates. [75]

After deciding the phase of the water present in all streams, the partial pressure CO_2/H_2S ratio was calculated. By calculating this ratio it could be concluded whether the corrosion is of sour, mixed or sweet dominant type. To do so the partial pressure of carbon dioxide and hydrogen sulfide was calculated in the same way as for water, according to Equation 3.7.

All values for temperature, pressure and composition of HCl, NH_3, H_2S, CO_2 and H_2O, used in the calculations presented in Sections 3.4 and 3.5, was simulated by Haldor Topsoe as a request by Preem when co-processing 20 wt% or more of rapeseed oil together with a balanced amount of LAGO.

4 Results & Discussion

The results presented in this section are divided into free fatty acid, aqueous and ammonium salt corrosion. For free fatty acid corrosion the TAN results of the twelve heat treated samples and the three reference samples are presented. The given results shows how the TAN values differs between temperatures and mixtures of rapeseed oil and how these results relate to the LAGO run through the SynSat unit before the revamp. The given values are also presented as corrosion rates of ASS alloys 321, 316 and 317L.

This section also gives a summary of theoretical kinetic calculations in a hydrogen-free environment. Correlations and comparison between the laboratory values for corrosion rates and theoretical corrosion rates is then given. The section also presents the results from the aqueous corrosion and ammonium salt corrosion studies in the amine recovery system. With further explanation and discussions on the importance of the presence of water.

4.1 Analysis of acid number

Depending on the expected TAN values for the samples, the sample weight had to be adjusted. The higher TAN value expected, the less amount of sample is required. Therefore the sample weight between the different samples can differ. This is done to obtain as representative and reproducible results as possible, reducing any sources of error when excessive or small amount of KOH is needed. Such a desirable interval of added KOH lies between 2 - 8 ml. The values presented in this section only covers values from ± 2 5mV from the fixed point which were set to -134.3 mV. Therefore the first endpoint of all samples is not shown in any table. Other values outside of this interval does not have any value of interest for the measurements and is not shown.

4.1.1 Analysis at 290°C

From Table 4.1 the voltage and added volume of KOH for Samples 1 - 4 is shown. The values were taken from the results obtained in Figures 4.1 - 4.4. Notice that the samples was added by different sample volumes, varying from 5 - 7 g, depending on its expected TAN value. Endpoints and fixed point are taken from the graphs and are translated according to Equation 3.1 with the total acid number values being shown in Table 4.2.

Table 4.1: *TAN analysis for Sample 1 - 4 (at 290 °C).*

Sample	EP2 [mV]	EP2 [ml]	FP [mV]	FP [ml]
1	-115.1	2.543	-134.3	2.703
2	-	-	-134.3	2.652
3	-	-	-134.3	2.602
4	-139.0	1.950	-134.3	1.919

In Figure 4.1 Sample 1 is presented. From the graph two endpoints and one fixed point can be observed. Since the voltage value of the first endpoint (EP1) lies significantly more than ± 25 mV from the fixed point, it can be seen as a ghost point and should not be taken in consideration when determining the TAN value. Endpoint number two (EP2) lays -19.2 mV from the fixed point and therefore represent the TAN value of Sample 1. From the calculations of the second endpoint from Table 4.1 a TAN value of 0.10 mg KOH/g is given.

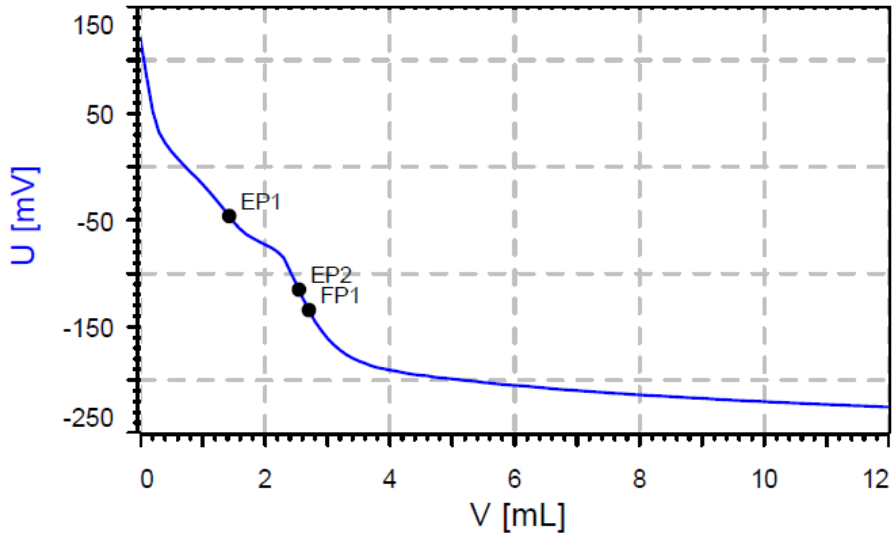

Figure 4.1: *TAN analysis of Sample 1.*

The graph for TAN analysis of Sample 2 is presented in Figure 4.2. From this graph two endpoints together with one fixed point can be observed. Both of the two endpoints have a voltage value of more than ± 25 mV from 134.3 mV. In this case where both endpoints lie more than ± 25 mV from -134.3 mV, the value of the fixed point (0.13 mg KOH/g) is the TAN value for Sample 2.

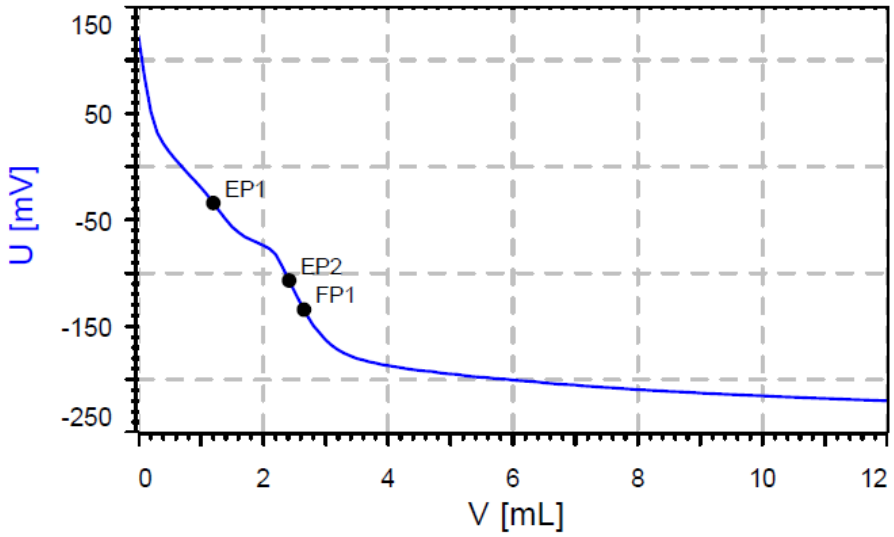

Figure 4.2: *TAN analysis of Sample 2.*

In Figure 4.3, the graph for Sample 3 is presented. The result of the graph shows to be similar to the two previous curves for 290 °C. Here the first endpoint also is a ghost point whereas the second end point lies -33.7 mV from the fixed point. Therefore, the fixed point is chosen as the accurate TAN value, giving a value of 0.15 mg KOH/g.

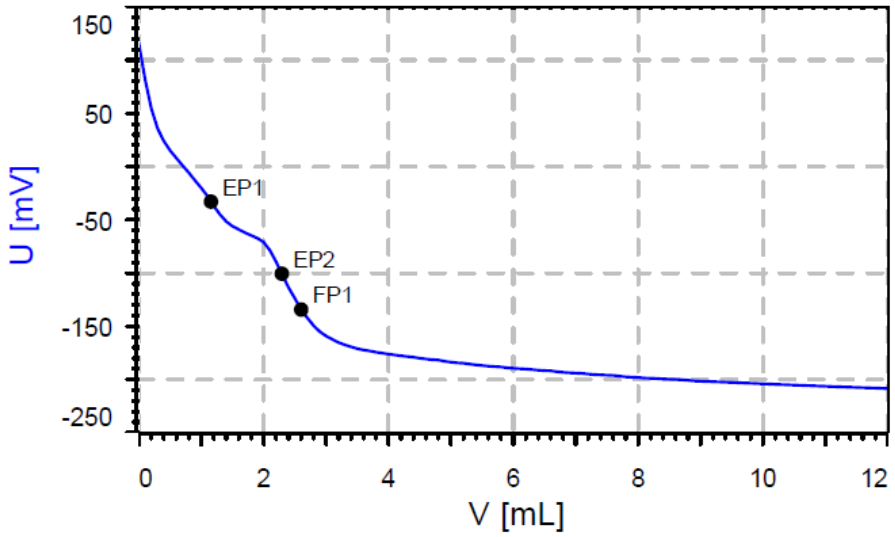

Figure 4.3: *TAN analysis of Sample 3.*

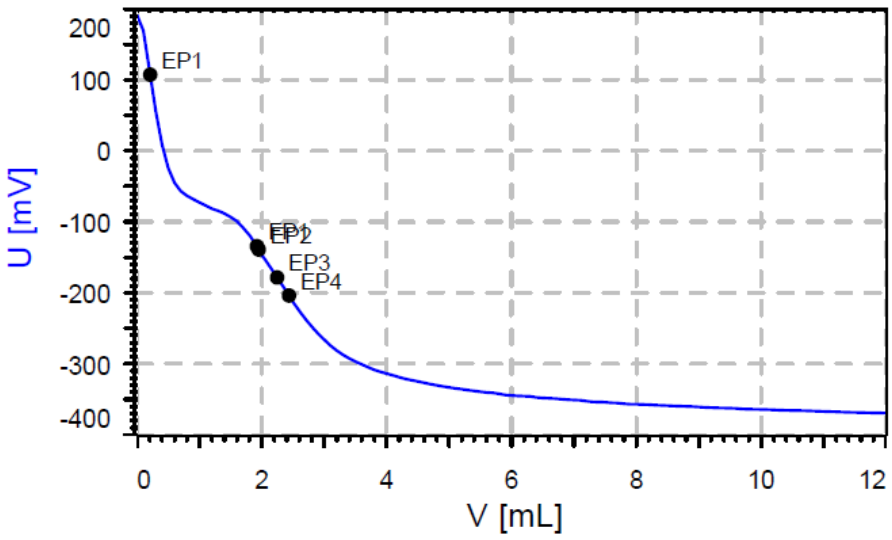

Figure 4.4: *TAN analysis of Sample 4.*

The last sample heated to 290 °C is Sample 4 containing 100 wt% of rapeseed oil, seen in Figure 4.4. Here a total of four endpoints has been measured. Only one of them lies within the interval of ± 25 mV from the fixed point. This is the second endpoint (EP2) with a measured voltage of -139.0 mV. This value is given as 0.56 mg KOH/g in Table 4.2.

When comparing the results of the four different mixtures of LAGO and rapeseed oil at 290 °C (Samples 1 - 4) one can see, as expected, that a higher wt% of rapeseed oil provides a higher value of TAN. In Table 4.2 a summary of the TAN values for all the accurate points (EP2 and FP) has been compiled. Bold marked values are the values accurate for the different samples whereas the other acid number gives the value for the points not chosen. One can clearly see from this table that TAN does increase with increased addition of rapeseed oil, but rather insignificantly for 5, 10 and 15 wt%. The value standing out is, unsurprisingly, Sample 4 with a significantly higher TAN value.

Table 4.2: *Acid Number for Sample 1 - 4 (at 290 °C). Bold marked values are the TAN value chosen.*

Sample	EP2 [mg KOH/g]	FP [mg KOH/g]
1	**0.10**	0.11
2	0.11	**0.13**
3	0.12	**0.15**
4	**0.56**	0.54

4.1.2 Analysis at 310°C

Samples heated to 310 °C includes Samples 5 - 8. The measured result of these samples are presented in Table 4.3 and the TAN values in Table 4.4. Comparing Table 4.1 with Table 4.3 it can be seen that at the same amount of wt% rapeseed oil and sample weight for each wt%, the added volume of KOH is significantly larger at 310 °C. When comparing 5 wt% of rapeseed oil between the two temperatures of 290 and 310 °C there is a voltage difference of 18.4 mV and for 100 wt% of rapeseed oil a difference of 9.2 mV. This indicates that for Samples 5 - 8 a higher TAN should be expected than for Samples 1 - 4, according to Equation 3.1.

Table 4.3: *TAN analysis for Sample 5 - 8 (at 310 °C).*

Sample	EP2 [mV]	EP2 [ml]	FP [mV]	FP [ml]
5	-149.1	4.257	-134.3	4.155
6	-133.6	4.237	-134.3	4.242
7	-129.9	4.018	-134.3	4.047
8	-148.2	2.862	-134.3	2.741

The values of Table 4.3 are taken from Figure 4.5 - 4.8. The graph of the TAN analysis for Sample 5 is presented in Figure 4.5. What is clear to see in this graph is that the first endpoint is a ghost point, according to the reasons described in section 4.1.1, whereas the second endpoint and the fixed point are staying close to each other with a difference of only 14.8 mV. Since the difference is less than ± 25 mV, the second endpoint provides TAN value to be 0.23 mg KOH/g for Sample 5.

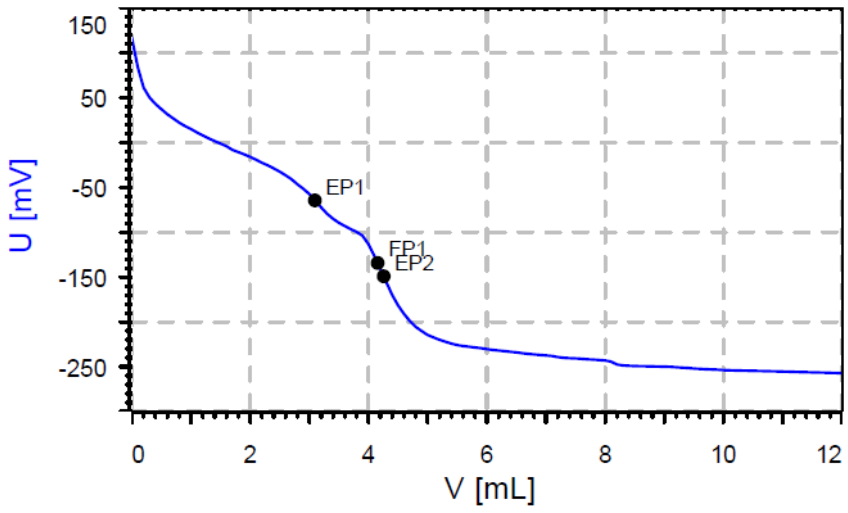

Figure 4.5: *TAN analysis of Sample 5.*

For Sample 6, see Figure 4.6, the second endpoint lies very close to the fixed point (-133.6 mV and -134.3 mV respectively). With these two points in close proximity of each other the same TAN result is to be expected. Reading from Table 4.4 one can see that this is the case with a TAN value of 0.27 mg KOH/g.

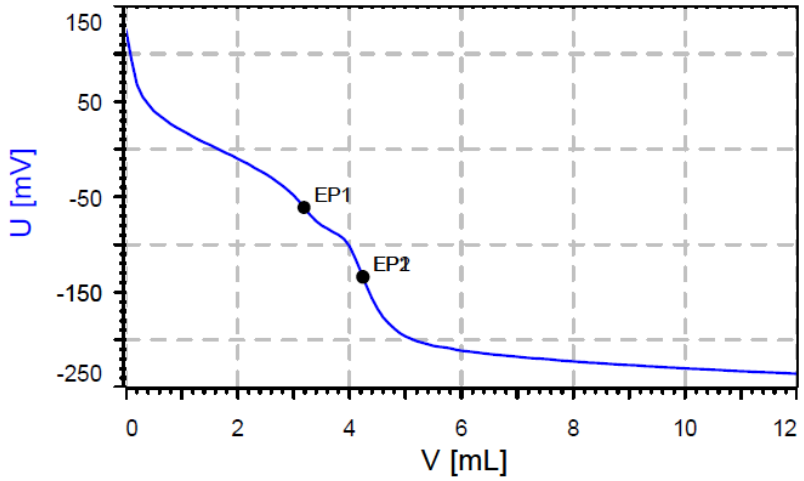

Figure 4.6: *TAN analysis of Sample 6.*

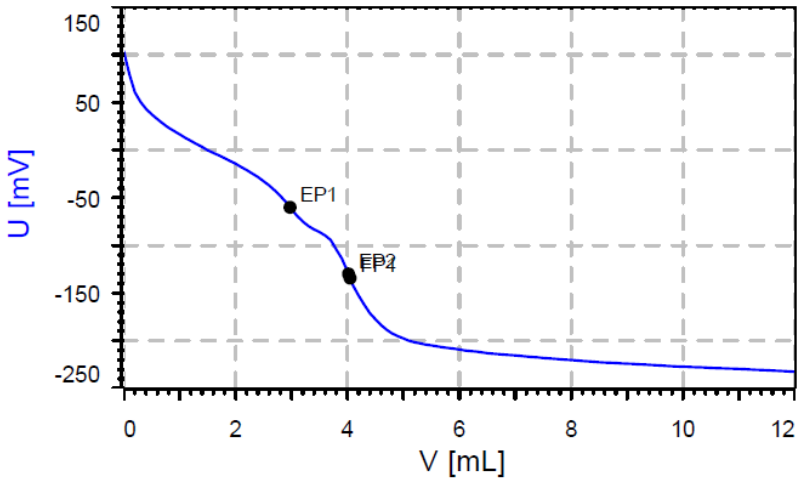

Figure 4.7: *TAN analysis of Sample 7.*

For Sample 7 the endpoints and fixed point can be seen in Figure 4.7. As in Figure 4.6 and the other presented graphs the first endpoint stands as a ghost point. However, the second endpoint of 129.9 mV stays very close to the fixed point of 134.3 mV. Therefore the

value of the second endpoint is chosen as TAN value for Sample 7, being 0.29 mg KOH/g.

The last sample heat treated at 310 °C is Sample 8. During the TAN measurement of this sample a numerous amount of endpoints has been found, see Figure 4.8. It is however only the second endpoint laying in the interval of ± 25 mV. From EP2 a TAN value of 0.75 mg KOH/g is given.

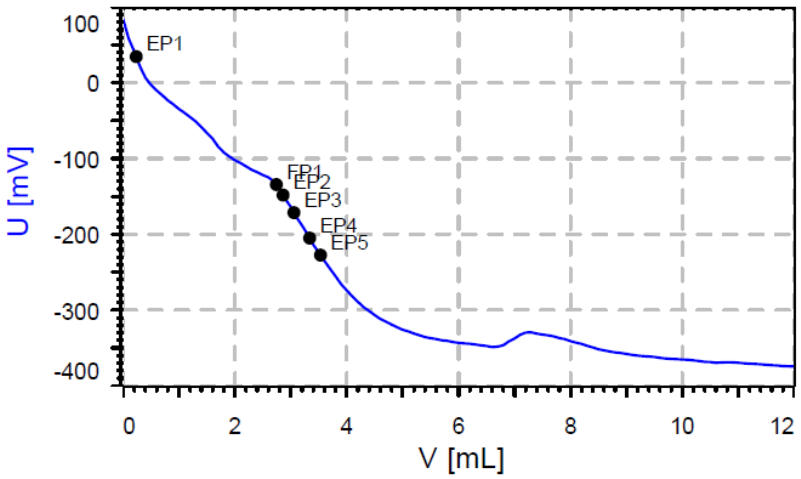

Figure 4.8: *TAN analysis of Sample 8.*

Comparing Table 4.4 with Table 4.2 one can observe a clear increase in the TAN. The TAN analysis for a mixture of 5 wt% rapeseed oil varied from 0.10 mg KOH/g to 0.23 mg KOH/g by only an increase of 20 °C. It can be concluded from these results that an increase in temperature has a larger impact than the wt% of rapeseed oil for these two temperatures. The difference from 5 wt% to 15 wt% of rapeseed oil for 290 °C is 0.05 mg KOH/g whereas for 310 °C it is 0.06 mg KOH/g which are small differences when discussing risk of corrosion. Comparing 100 wt% rapeseed oil (Sample 4 and 8) at 290 °C and 310 °C a difference of 0.19 mg KOH/g is shown.

Table 4.4: *Acid Number for Sample 5 - 8 (at 310 °C). Bold marked values are the TAN value chosen.*

Sample	EP2 [mg KOH/g]	FP [mg KOH/g]
5	**0.23**	0.22
6	**0.27**	0.27
7	**0.29**	0.29
8	**0.75**	0.69

4.1.3 Analysis at 330°C

The highest temperature investigated when heat treating the samples was 330 °C which results will be presented in this section. All endpoint values seen in Table 4.5 lies inside the ± 25 mV interval from the fixed point and is presented both as voltage and added KOH in order to neutralize the sample. Therefore some values for different endpoints for Samples 10 and 11 are missing due to values outside of this ± 25 mV interval. Having values outside of the interval makes values of the fixed point the accurate TAN value. All such values are presented later in this section in Table 4.6.

Table 4.5: *TAN analysis for Sample 9 - 12 (at 330 °C).*

Sample	EP1 [mV]	EP1 [ml]	EP2 [mV]	EP2 [ml]	FP [mV]	FP [ml]
9	-	-	-158.5	4.587	-134.3	4.299
10	-	-	-	-	-134.3	4.598
11	-	-	-	-	-134.3	5.102
12	-129.8	6.535	-	-	-134.3	6.591

Sample 9 containing 5 wt% rapeseed oil heated to 330 °C is presented in Figure 4.9. When comparing the graphs of the 5 wt% rapeseed oil samples for the different temperatures one can observe that the two at lower temperature (290 °C and 310 °C) only have two endpoints whereas at 330 °C has four endpoints. It is however only the second endpoint which lies in the ± 25 mV interval from the fixed point giving a TAN value of 0.9 mg KOH/g.

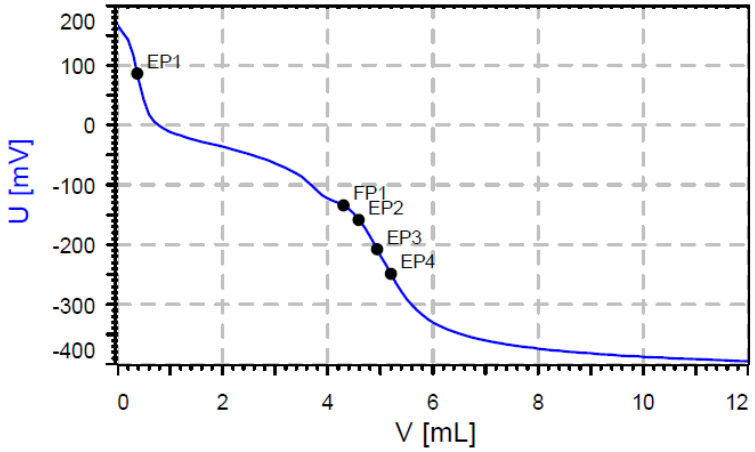

Figure 4.9: *TAN analysis of Sample 9.*

Figure 4.10 represent the 10 wt% rapeseed oil sample at 330 °C. The two endpoints on the curve lies far away from the fixed point of -134.3 mV, close to 200 mV. Therefore none

of the endpoints can be used with Equation 3.1 to obtain an accurate TAN value for the sample. Instead, as in previous samples where no endpoint lay in the ± 25 mV interval from the fixed point, the value of the FP itself had to be chosen to calculate TAN. From the calculations TAN was decided to 0.9 mg KOH/g.

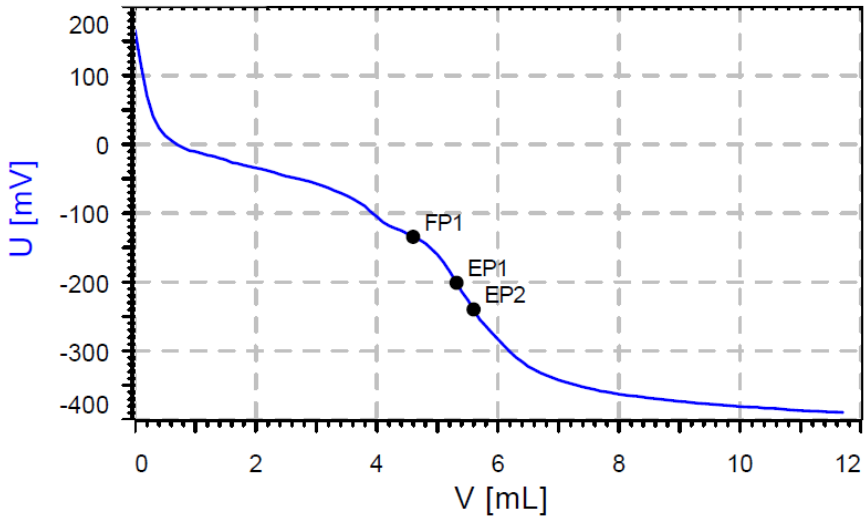

Figure 4.10: *TAN analysis of Sample 10.*

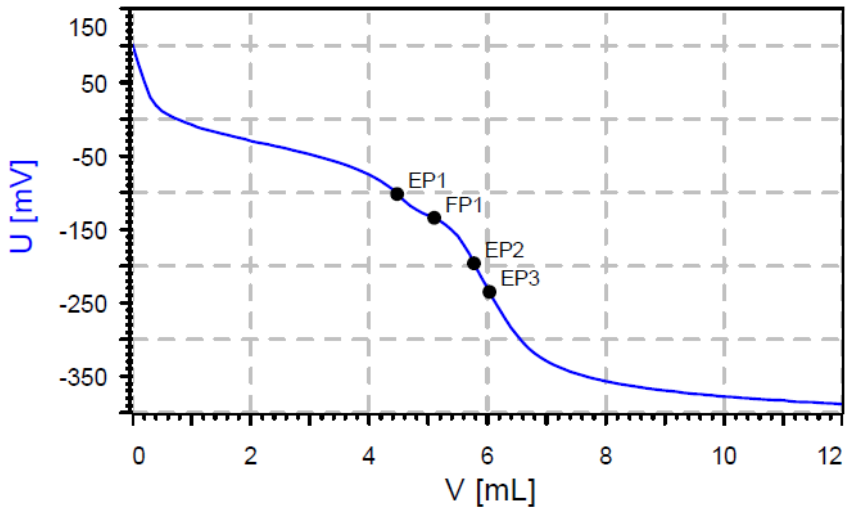

Figure 4.11: *TAN analysis of Sample 11.*

The graph for Sample 11 is presented below in Figure 4.11 with three endpoints and one fixed point. Although since all of the three endpoints lie outside of the ± 25 mV

interval they are not of interest when deciding the TAN value for this sample. Instead the calculated values from the fixed point should be used, giving a TAN value of 1.03 mg KOH/g.

The last graph presented in this section is the one for Sample 12, see Figure 4.12. From the figure is can clearly be seen that the endpoint and the fixed point lies very close to each other (-129.8 mV and -134.3 mV respectively). Therefore the second endpoint is used with Equation 3.1 to obtain the TAN value.

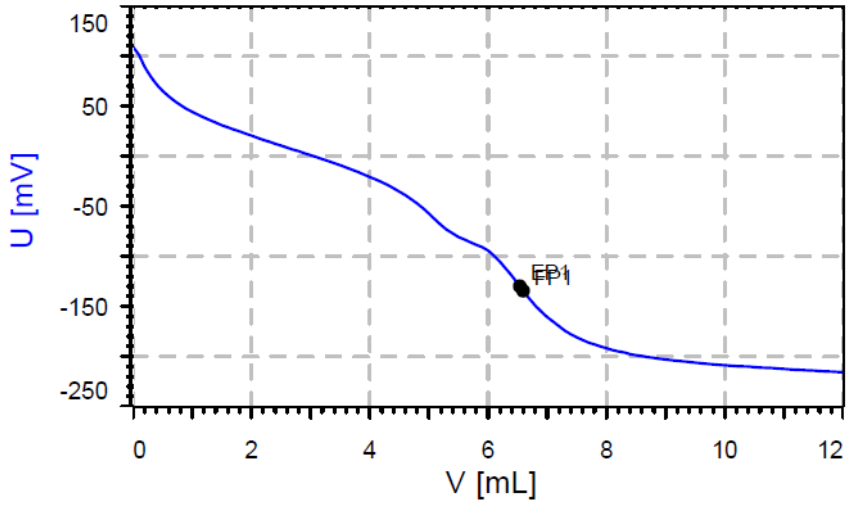

Figure 4.12: *TAN analysis of Sample 12.*

As in the previous measurements at 290 °C and 310 °C the impact of added rapeseed oil between 5 - 15 wt% is rather low with a total difference of 0.13 mg KOH/g, see Table 4.6. What might come as more interesting is the step between 15 to 100 wt% rapeseed oil where the later has a TAN value as high as 2.55 mg KOH/g. Values this high will show risk of fatty acid corrosion in the SynSat unit.

Table 4.6: *Acid Number for Sample 9 - 12 (at 330 °C). Bold marked values are the TAN value chosen.*

Sample	**EP1** [mg KOH/g]	**EP2** [mg KOH/g]	**FP** [mg KOH/g]
9	-	**0.90**	0.82
10	-	-	**0.90**
11	-	-	**1.03**
12	**2.55**	-	2.58

4.1.4 Reference analysis

In order to analyze the given sample results from heat treatment at 290, 310 and 330 °C it is of great importance to have reference values. Such values were presented in Section 3.2 as Sample 13 - 15. The reference analysis was taken at room temperature (25 °C) without the samples undergoing any heat treatment. Measured values of TAN for the reference samples are shown in Table 4.7.

Table 4.7: *TAN analysis for Sample 13 - 15 (at 25 °C).*

Sample	EP3 [mV]	EP3 [ml]	EP4 [mV]	EP4 [ml]	FP [mV]	FP [ml]
13	-124.8	2.167	-153.8	2.386	-134.3	2.240
14	-124.4	2.235	-148.3	2.418	-134.3	2.304
15	-131.3	2.189	-	-	-134.3	2.210

In Figure 4.13 a closer look of the graph for Sample 13 is presented. In the graph both the first and the second endpoint are ghost points whereas endpoints three and four lie rather close to the fixed point of the sample. Both endpoints stay in the interval of ± 25 mV from the fixed point value of -134.3 mV, with EP3 higher than FP and EP4 lower than FP. Therefore, the fixed point, lying in the middle of the two endpoints best represent the TAN value of Sample 13. The obtained value of 0.06 mg KOH/g is rather low, especially in comparison with the TAN values of the heat treated samples with 5 wt% rapeseed oil (Sample 1, 5 and 9).

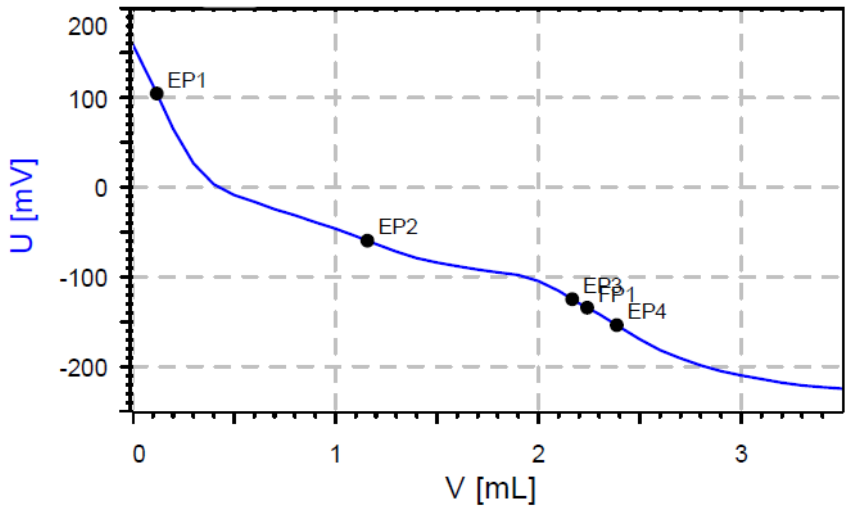

Figure 4.13: *TAN analysis of Sample 13.*

Analyzing Figure 4.14, similarities with Figure 4.13 are rather clear. As for Sample 13 both the first and the second endpoints stays as ghost points whereas the third and fourth

endpoints lies close (in the interval of ± 25 mV) to the fixed point of -134.3 mV.

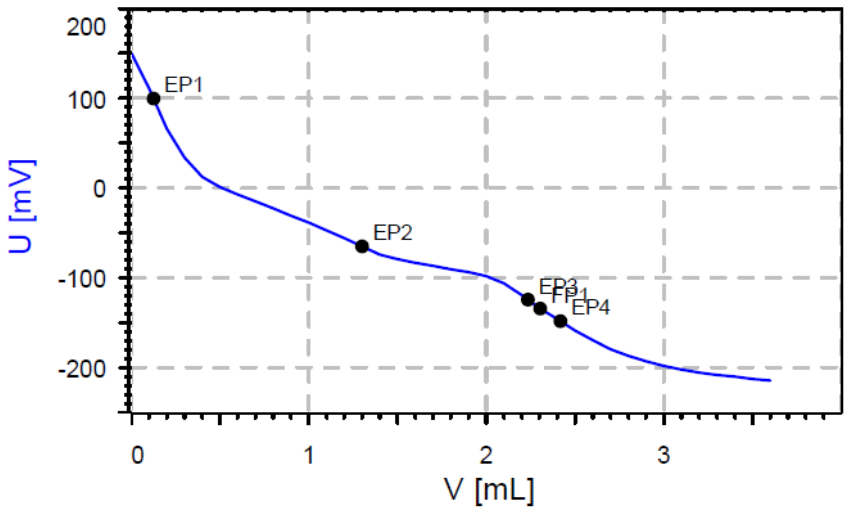

Figure 4.14: *TAN analysis of Sample 14.*

Therefore when choosing a representative TAN value of the sample, the fixed point staying in between the two endpoints are chosen giving a TAN value of 0.06 mg KOH/g. All the points of EP3, EP4 and FP also stays within the desirable interval of 2 - 8 ml added KOH.

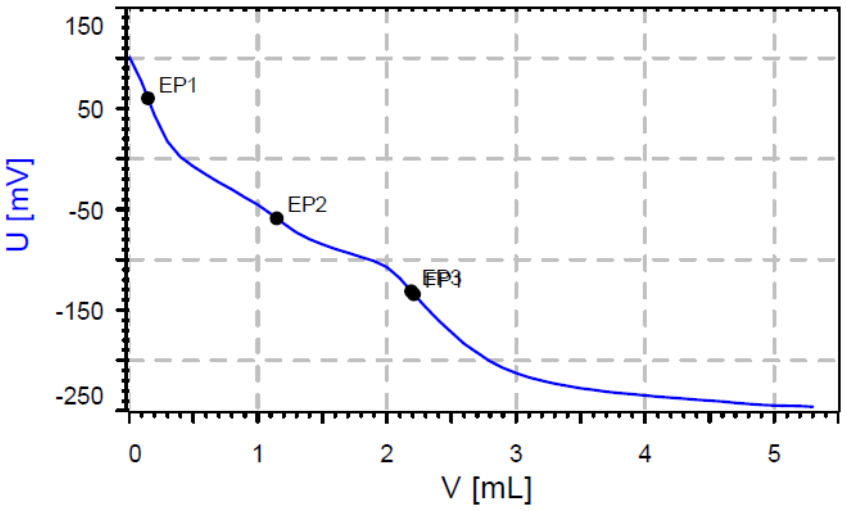

Figure 4.15: *TAN analysis of Sample 15.*

Sample 15 is represented by Figure 4.15 where endpoint three and the fixed point gives an almost identical value. EP3 is therefore chosen which gives a TAN of 0.05 mg KOH/g.

In Table 4.8 a summary of the TAN values for the first, second and third endpoints together with the fixed points are presented for the reference samples. Values marked bold are the representative TAN values of each sample. When comparing the values between the samples and thus the different blends of rapeseed oil one can conclude that different wt% of rapeseed oil does not significantly effect the TAN results in room temperature.

Table 4.8: *Acid Number for Sample 13 - 15 (at 25 °C). Bold marked values are the TAN value chosen.*

Sample	EP3 [mg KOH/g]	FP [mg KOH/g]
13	0.05	**0.06**
14	0.05	**0.06**
15	**0.05**	0.05

4.2 Comparison of acid number

In this section, the TAN values presented in Section 4.1 are compared with each other in order to study potential patterns. Both by comparing the effect of added wt% at same temperature but also by observing different trends between the added wt% of rapeseed oil at different temperatures.

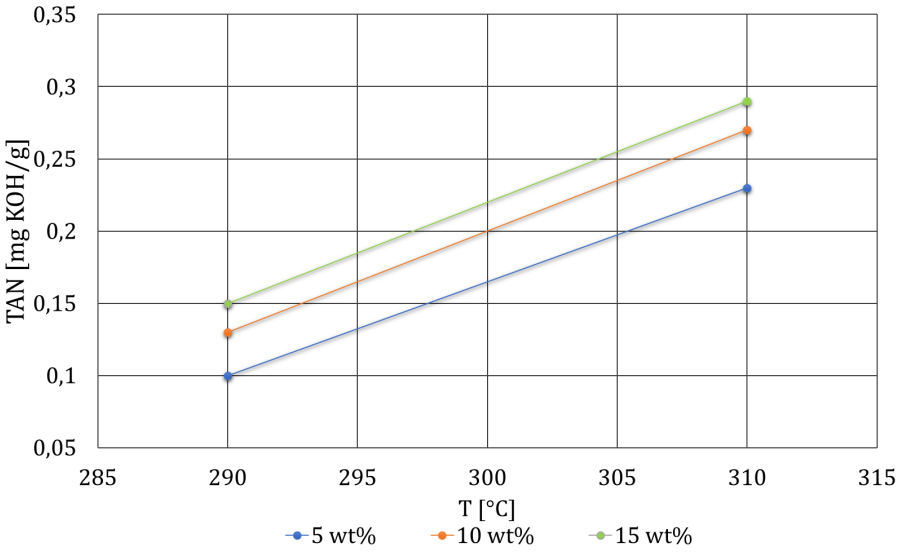

Figure 4.16: *Impact on TAN when co-processing 5, 10 and 15 wt% rapeseed oil between 290 and 310 °C.*

A comparison between the added wt% of rapeseed oil, when co-processing it with LAGO at 290 and 310 °C is seen in Figure 4.16. Observing the curves for each wt% one can see that they all follow the same trend with an increase of ~14 mg KOH/g from 290 to 310 °C when heated. When analyzing these values with respect to the two temperatures it can be concluded that an increase in TAN, and hence decomposition of fatty acids into free fatty acids, is rather small. All values, regardless of added wt% or temperatures lies far below any value that may cause a risk of corrosion. It can thereby be concluded that co-processing 15 wt% rapeseed oil, or less, balanced with LAGO up to a temperature of 310 °C, no concern for corrosion has to be taken. Corrosion rates for the different samples will further explained in Section 4.3.

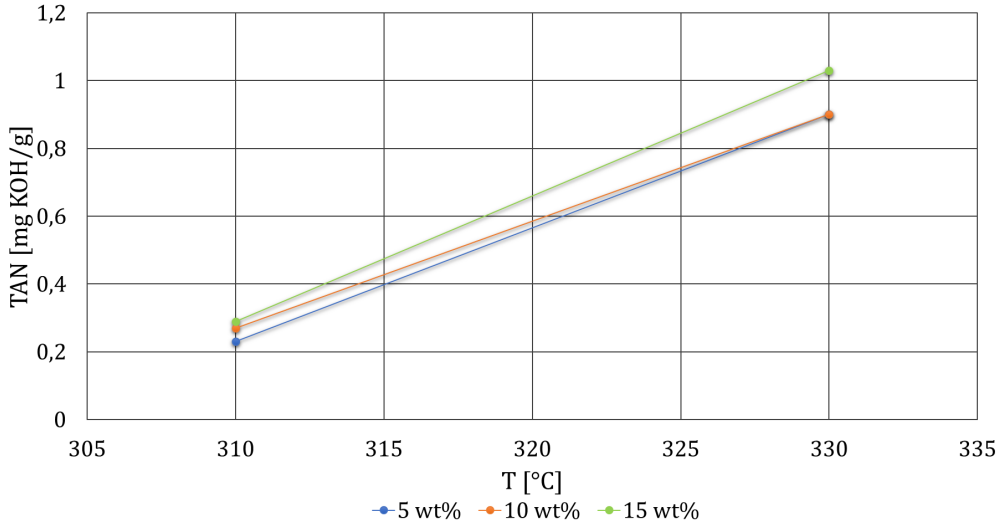

Figure 4.17: *Impact on TAN when co-processing 5, 10 and 15 wt% rapeseed oil between 310 and 330 °C.*

With the knowledge that a mixture of 5, 10 or 15 wt% of rapeseed oil balanced with LAGO at 290 and 310 °C does not have a significant effect of corrosion on stainless steel materials a further analysis of temperature up to 330 °C can be seen in Figure 4.17.

All three wt% increases with 0.67 (5 wt%), 0.63 (10 wt%) and 0.74 mg KOH/g (15 wt%) respectively. Comparing the difference in TAN values between 290 to 310 °C and 310 to 330 °C a substantial larger increase can be seen in the latter. Hence, the conclusions indicate that the amount of released unsaturated free fatty acids from triglycerides is significantly higher above 310 °C than at lower temperatures.

The amount of rapeseed oil will continuously be increased in the coming years. Therefore, it is also of interest to observe the values of Sample 4, 8 and 12 at 100 wt% rapeseed oil without any fossil feed. Such data point are shown with a combination with the values showed in Figure 4.16 and 4.17 in Figure 4.18.

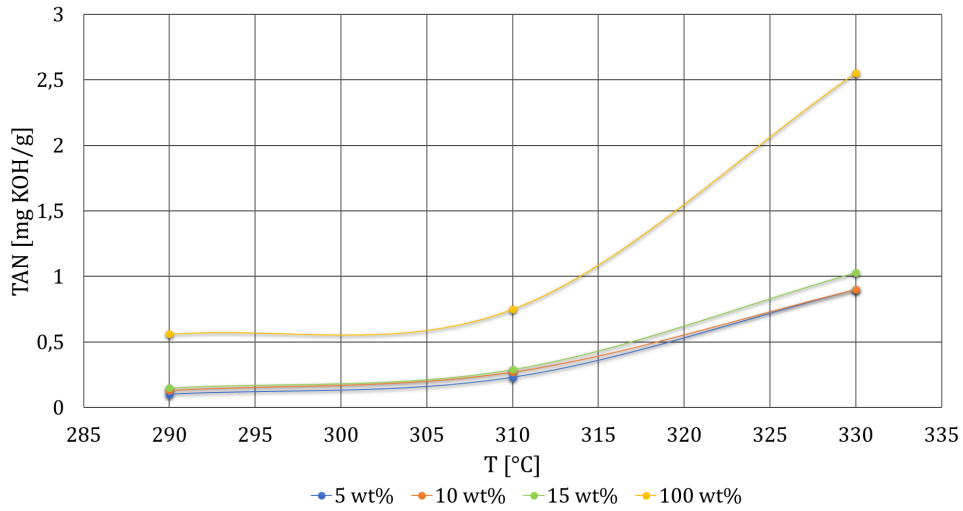

Figure 4.18: *Impact of TAN when co-processing 5, 10, 15 and 100 wt% rapeseed oil over temperature interval of 290 to 330 °C.*

From this graph it can clearly be seen that 100 wt% of rapeseed oil has a higher TAN value at 290 °C in comparison to the blended rapeseed oil samples. It does, however, follow the trend to these blended samples up to a temperature of ~310 °C. At temperature 330 °C Sample 12 does not longer follow the trend according to Samples 3, 7 and 11 but has increased greatly in comparison to the other samples. All trends can be seen more clearly in Figure 4.18. It can therefore be concluded that the decomposition of triglycerides into free fatty acids, and hence an increase of corrosion, is rapidly increasing at temperatures around 310 - 330 °C.

4.3 Corrosion rates

The given results in Section 4.1 and 4.2 will, in this section, be correlated to the corrosion rates of the different samples. All corrosion rates values are based on tables in API 581 with focus on high temperature sulfidic and naphthenic acid corrosion. [76] When reading the corrosion rate from the tables some assumptions was done. These includes the wt% of sulfur in the mixed samples, which was set to 1.5 wt%. A total sulfur content of 1.5 wt% is higher then the expected value for the feed. Feeds run at a daily basis in the SynSat unit rather have a sulfur content of < 0.5 wt%. The value of 1.5 wt% was chosen in order to have a large margin in the calculations for corrosion rates.

For Samples 1 - 4, they are all estimated to have a corrosion rate of < 0.03 mm/year. This value is estimated from a temperature of 288 °C and the piping material being of austenitic stainless steel without Mo (*eg. SS alloy 321*) according to the API 581 table. [76] This value is of no considerable concern with regard to corrosion

The same corrosion rate value of < 0.03 mm/year is used for all samples heated to 310

°C (Samples 5 - 8). Conditions were identical as described above with a difference of temperature to 315 °C read out of the API 581 table. [76]

For the samples heated to 330 °C (Sample 9 - 12) estimated corrosion rate is set to < 0.03 mm/year for Sample 9 - 10 with a table temperature value of 343 °C. Sample 11 had a corrosion rate value of 0.03 mm/year and Sample 12, containing 100 wt% rapeseed oil had an estimated corrosion rate of < 0.08 mm/year. [76] Neither of Samples 1 - 12 induce any considerable risk of corrosion on stainless steel alloy 321 material, and are thereby of little concern to Preem.

With the same sulfur content (1.5 wt%) SS 316 and SS3 17L was tested for the different samples with the result showed in Table 4.9.

Table 4.9: *Corrosion rates for different stainless steel materials.* [76]

Sample	SS 321 [mm/year]	SS 316 [mm/year]	SS 317L [mm/year]
1	< 0.03	<0.03	<0.03
2	< 0.03	<0.03	<0.03
3	< 0.03	<0.03	<0.03
4	< 0.03	0.03	<0.03
5	< 0.03	0.03	<0.03
6	< 0.03	0.03	<0.03
7	< 0.03	0.03	<0.03
8	< 0.03	0.03	<0.03
9	< 0.03	< 0.08	<0.03
10	< 0.03	< 0.08	<0.03
11	0.03	< 0.08	<0.03
12	< 0.08	< 0.08	<0.03

From the table above one can conclude that the current material of stainless steel alloy 321 is a suitable choice when co-processing 5, 10 or 15 wt% rapeseed oil together with a balanced amount of LAGO. None of the tested samples showed considerable risk of corrosion. The least suitable choice of the three investigated stainless steel materials is alloy 316 which shows in higher corrosion rate than the other two materials, mainly at 330 °C. Alloy 317L would be the best choice due to its low corrosion rate but with the planned process parameters and added amount of rapeseed oil it is unnecessary, unwarranted and costly to change the pipe material.

4.4 Kinetic calculations

The given results in Section 4.1 and 4.2, implied in low TAN values when co-processing rapeseed oil. Thereby it is a low risk of corrosion on the inlet pipe before the HDS reactor. To prove that the inlet point of rapeseed oil however is placed correctly, the importance of hydrogen gas for degradation of triglycerides was calculated. Therefore a thermal

degradation study on the triglycerides in a hydrogen-free environment was performed.

In Figure 4.19 the degradation of triglycerides at 290 °C without hydrogen atmosphere is shown. The blue line represent triglycerides before degradation, whereas orange, green and yellow lines represent different steps in the degradation process. At a process temperature of 290 °C the calculations gave a degradation from 1.00 M to 0.85 M after 87 s, which represent the time it takes for the feed to reach the internal distributor at the top of the HDS reactor. A concentration of 0.85 M of triglycerides in the feed system represents a TAN value of 39 mg KOH/g, which is significantly larger than the TAN values calculated in Section 4.1

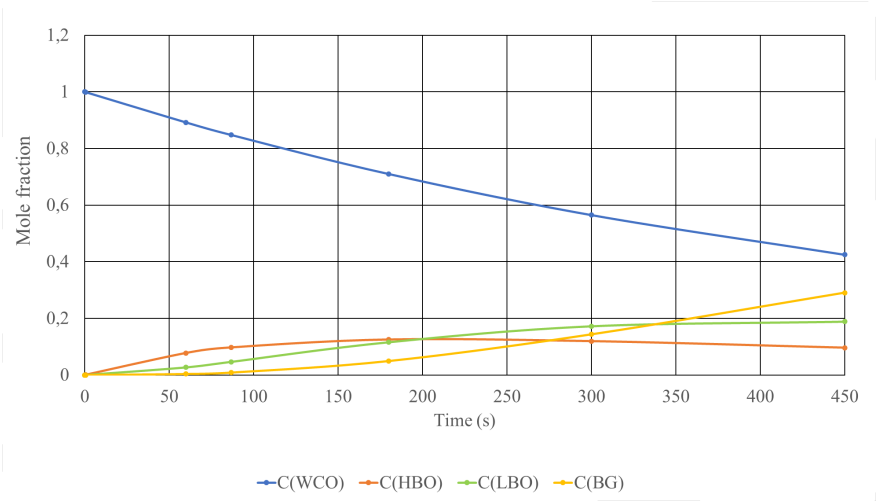

Figure 4.19: *Degradation of triglycerides at 290 °C in a hydrogen-free atmosphere.*

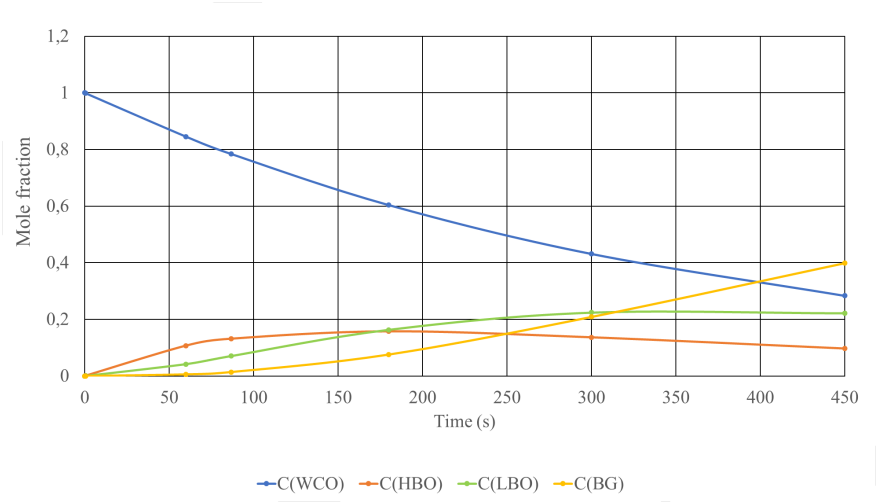

Figure 4.20: *Degradation of triglycerides at 310 °C in a hydrogen-free atmosphere.*

The thermal degradation at 310 °C without hydrogen atmosphere is presented in Figure 4.20. Here the initial concentration of 1.00 M triglycerides have decreased to 0.78 M at 87 s. This value represent a TAN value of 39 mg KOH/g.

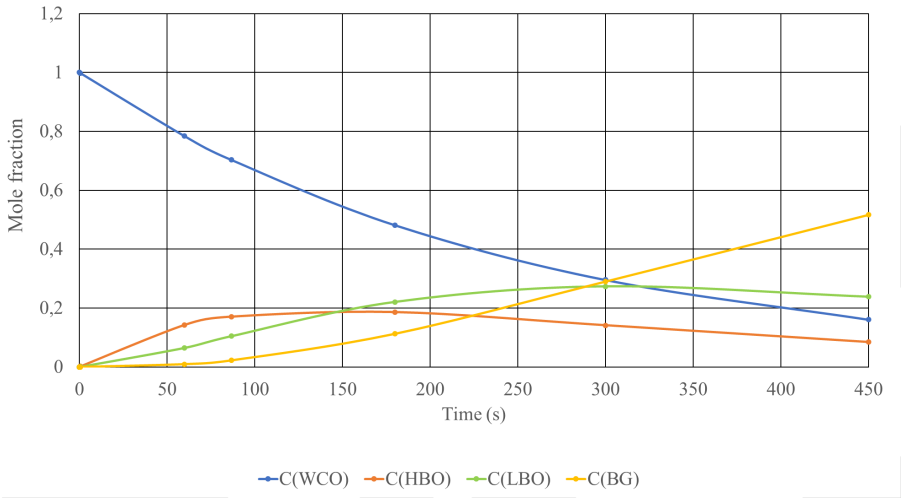

Figure 4.21: *Degradation of triglycerides at 330 °C in a hydrogen-free atmosphere.*

Thermal degradation of triglycerides at 330 °C are presented in Figure 4.21. Here it is clear to see that the degradation is rapidly increasing when comparing with Figure 4.19 and 4.20. After 87 s the remaining concentration of triglycerides is down to 0.70 M and a calculated TAN value of 54 mg KOH/g is given. A general trend of the diagrams is an increasing degradation when increasing temperatures. When comparing the TAN values from this theoretical calculations in a hydrogen-free environment with the measured TAN values in Section 4.1, a significant difference can be seen. It can therefore be concluded that the effect of hydrogen atmosphere is of great importance on thermal degradation of triglycerides. Therefore the rapeseed oil has to be added after the addition of recycled hydrogen gas in order to avoid a large risk of corrosion. After the addition of hydrogen gas it will chemically react and saturate with the feed of LAGO, and later rapeseed oil. With the results from Figure 4.19 - 4.21 implying that a high degradation of triglycerides is to be expected without hydrogen atmosphere, the position of the quill adding rapeseed oil to the unit is preferable after the addition of hydrogen gas as planned and installed by Preem.

4.5 Ammonium salt corrosion

The increased amount of chlorides in the renewable feedstock of rapeseed oil (> 12 ppm) in comparison with the fossil feed (< 1 ppm) makes the possibility of deposition of ammonium salt of great interest. If precipitates of salt crystals occurs, wash water has to be injected into the upstream system of the interstage stripper and HDA reactor.

To decide whether or not wash water injection is needed, the occurrence of deposition of salt crystals was calculated by deciding the salt stability constant for both ammonium chloride and ammonium bisulfide. The partial pressure values for each compound of NH_3, HCl and H_2S at stream A and E is presented in Table 4.10. Stream A represents the feed before the heat exchanger and air cooler, entering the HHPS. Whereas stream E represents the feed right before it enters the air cooler and then the CHPS. All streams were earlier presented in Figure 2.5.

What can be observed in Table 4.10 is that for stream E, the partial pressure for HCl is zero. This means that there should not be any compounds of HCl left in the feed as it has been separated and washed away in the HHPS. Therefore precipitates of ammonium chloride salt crystals is not be expected in streams E or F.

Table 4.10: *Partial pressure [psia] of NH_3, HCl and H_2S for stream A and E.*

	Stream A	*Stream E*
NH_3	0.053	0.036
HCl	0.004	0.0000
H_2S	2.311	2.393

With the absence of ammonium chloride salt crystals in stream E and F, the salt stability constant, K_{NH3Cl}, as can be seen in Table 4.11, is calculated to be zero. For ammonium bisulfide, a presence of salt deposit can be observed in both stream A and E, meaning it has not been separated and washed away completely. It can however be seen that the salt stability constant for ammonium bisulfide has decreased when comparing stream A with stream E.

Table 4.11: *Salt stability constant [$psia^2$] of NH_3, HCl and H_2S for stream A and E.*

	Stream A	*Stream E*
K_{NH_4Cl}	$1.89*10^{-4}$	0.00
K_{NH_4HS}	$1.22*10^{-1}$	$8.68*10^{-2}$

In order to predict whether or not a deposition of salt crystals of ammonium chloride and ammonium bisulfide can occur in the streams of A - F, the stream temperatures are of importance together with the already calculated salt stability constants for each compound and stream. All temperatures for streams A, B, C, E and F are shown in Table 4.12, where stream A have the highest temperature of 231 °C and stream F the lowest of 118 °C.

Table 4.12: *Stream temperature [°C] for stream A, B, C, E and F.*

	Stream A	*Stream B*	*Stream C*	*Stream E*	*Stream F*
Temperature [°C]	231	172	153	140	118

By knowing both the salt stability constant for ammonium chloride and ammonium bisulfide and the temperatures, the occurrence of deposition of the two ammonium salts could

be decided. The diagram in Figure 4.22 was created from the diagram shown in Figure A.2 in Appendix II. The dotted line at $1.89*10^{-4}$psia^2 represent the operating salt stability constant (K_{NH4Cl}) for stream A, B and C in the case without a water wash injection point between stream A and B. With the salt stability constant representing the partial pressure and hence the composition of NH_3 and HCl, the composition between the two compounds stays the same without a water injection point. The only parameter changing between the streams in this case is the temperature. Stream A with the highest temperature is represented by the blue dot in the diagram laying on the operating K_{NH4Cl} whereas stream B is represented by the orange dot and stream C by the green dot.

As can be observed from Figure 4.22, deposition of ammonium chloride is to be expected for temperatures < 170 °C. That makes both stream B and C candidates for deposition of ammonium chlorides, since they lie close or below this temperature and lack a water injection. The formation of ammonium chloride salt crystals increase risk of later fouling and corrosion to the pipes in heat exchangers and air coolers and is therefore undesired.

Since the salt stability constant for ammonium chloride in stream E was calculated to zero and is not expected in stream E or F, a diagram of deposition for ammonium chloride salt in these streams was not investigated further.

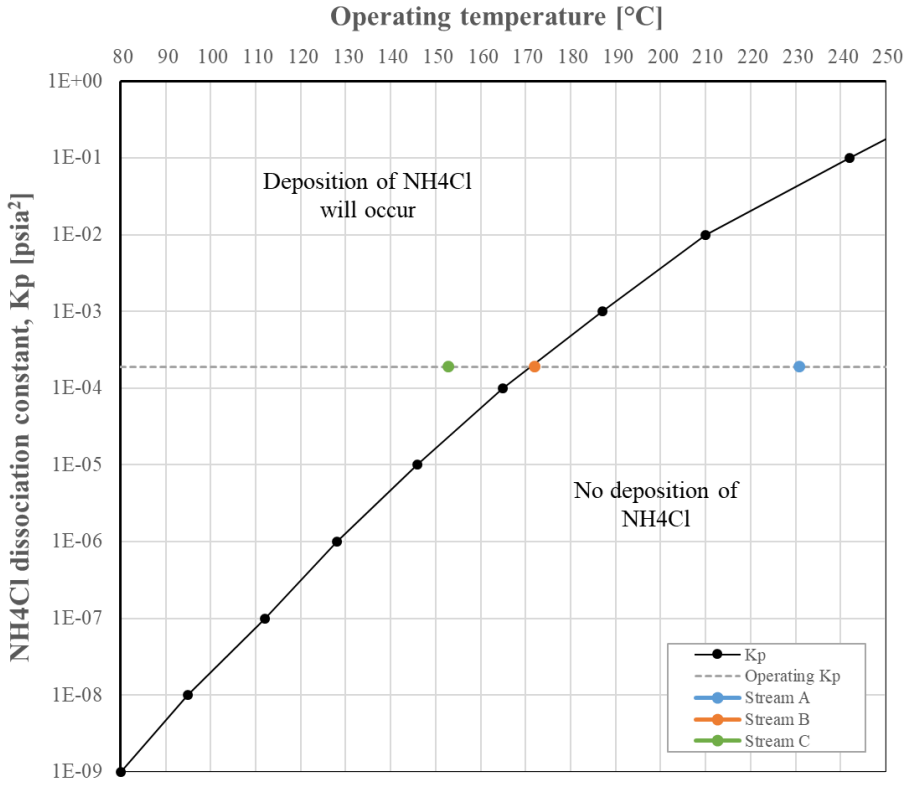

Figure 4.22: *Deposition of NH_4Cl salt for stream A,B and C (before the HHPS).*

With an ammonium bisulfide salt stability constant of $1.22*10^{-1}psia^2$ and $8.68*10^{-2}psia^2$ respectively for stream A and E both streams has to be investigated due to the possibility of salt deposition. Firstly stream A, B and C was investigated which can be seen in Figure 4.23. The diagram for deposition of ammonium bisulfide salt was created from Figure A.3 in Appendix II. As in Figure 4.22, the dotted line is represented by the operating salt stability constant of $1.22*10^{-1}psia^2$, which lies far below the critical salt stability line for each temperature of 231, 172 and 153 °C respectively. Therefore it can be concluded that no deposition of ammonium bisulfide is to be expected for stream A, B or C.

For stream E and F the salt stability constant of ammonium bisulfide is lower then for stream A, B and C. Observing the diagram for deposition of ammonium bisulfide salt it can be seen that a decrease in the salt stability constant must result in no deposition of ammonium bisulfide also for stream E and F. This is shown and presented more clearly in Figure 4.24.

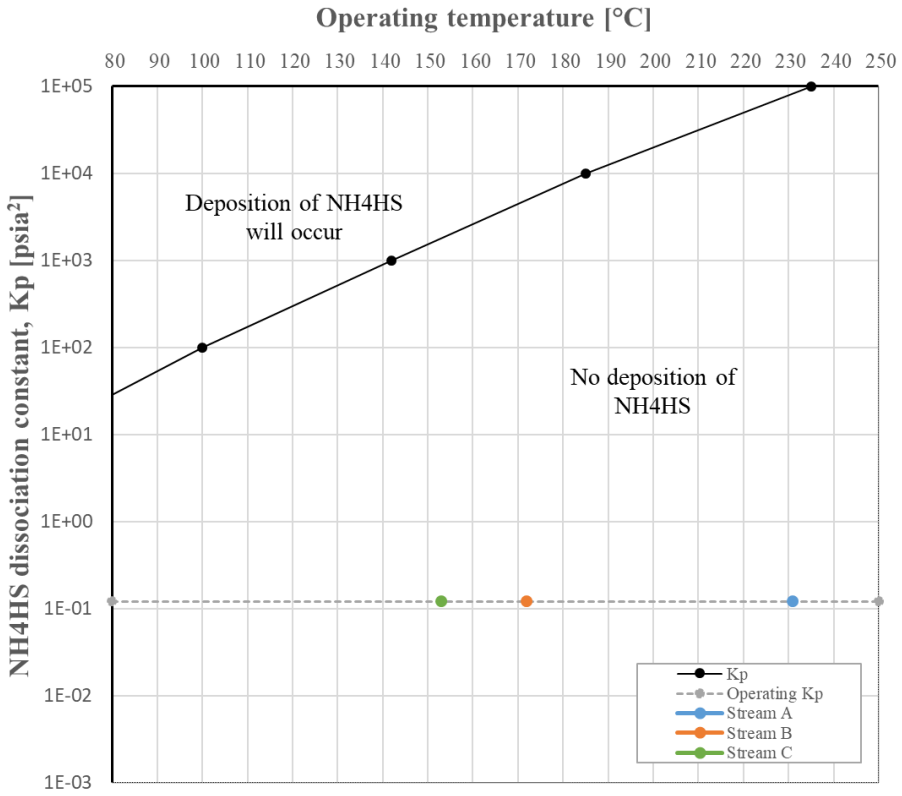

Figure 4.23: *Deposition of NH_4HS salt for stream A,B and C (before the HHPS).*

With the given results for deposition of ammonium chloride and ammonium bisulfide at the upstream system of the interstage stripper and HDA reactor it can be concluded that the first planned wash water injection (between stream A and B) is necessary in order to avoid the risk of formation of ammonium chloride crystals which later can cause fouling

and corrosion on the pipe materials on heat exchanger and air cooler. The second wash water injection point is an old, already present wash water injection point which will be intact even though its not necessary from a salt deposition point of view, after the revamp of the SynSat unit.

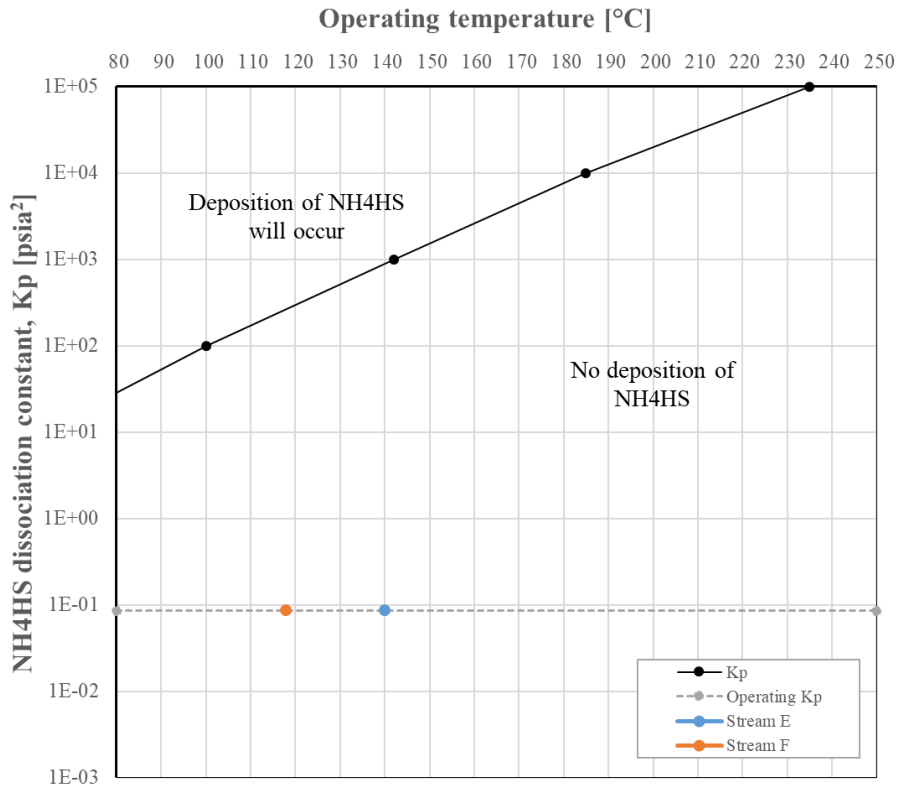

Figure 4.24: *Deposition of NH_4HS salt for stream E and F (before the CHPS).*

4.6 Corrosion prediction of H_2S and CO_2

4.6.1 Water phase

The risk of sour or sweet corrosion is most significant when the compounds makes a contact with liquid water which will be injected at two points in the amine recovery system. To understand such risk of corrosion the phase of water in the streams were calculated. This was done in several steps where firstly the partial pressure of water in the different streams are presented in Table 4.13. As described in the methodology, an assumption that the total feed stream was in completely vaporous phase was made. Instead the actual fraction of vapor, in mass basis, was 97% for stream A, 86% for stream B, 100% for stream E and 98% for stream F. The assumption of a complete vaporization of the whole stream was made because of the absence of data for which substances that were in vapor phase and which were in liquid phase for the accurate streams. The partial pressure value of water for the four streams is therefore only an estimation.

Table 4.13: *Calculated partial pressure for water in the amine recovery system.*

	Stream A	**Stream B**	**Stream E**	**Stream F**
Partial pressure [atm]	5.9	13.0	2.1	2.9

With the calculated partial pressure data of water for the four streams, a vapor pressure curve by Mörtstedt and Hellsten was used to find out the boiling temperature for each stream. [75] The provided results for the four streams are presented in Table 4.14 together with the operating temperatures.

Table 4.14: *Water boiling and operating temperature for the amine recovery system.*

	Stream A	**Stream B**	**Stream E**	**Stream F**
Boiling point temperature [°C]	160	190	125	135
Operating temperature [°C]	231	172	140	118

From Table 4.14 one can see that the boiling point temperature is less then the operating temperature for stream A and E and thereby no significant risk of corrosion is to be found in these streams. For stream B and F the boiling point temperature is higher than the operating temperature. Thereby the water is in liquid phase in these streams causing increased risk of H_2S and CO_2 corrosion.

With the results of water being in vapor phase in stream A and E and in liquid phase in stream B and F one can draw some conclusions. In stream A, which had a vapor fraction of 97%, there are other compounds then water being in vaporous phase. When then injecting water into stream B, one assumption could be that the added water represent 11% of the liquid fraction and other compounds represent the other 3%. When comparing stream E with stream F one can conclude that since all compounds in stream E are vaporized the water injection is the reason for stream F to reduce the vapor fraction by 2% to 98% vapor. Thereby these 2% are liquid water.

4.6.2 CO_2/H_2S ratio

From the given results in Section 4.6.1, showing in liquid water phase for stream B and F, the composition of the two streams had to be investigated. Therefore the partial pressure of carbon dioxide and hydrogen sulfide was calculated. In overall, the composition of carbon dioxide did not exceed 0.17 mole% whereas the hydrogen sulfide did not exceed 0.14 mole%. Composition values for each stream are shown in Table 4.15.

Table 4.15: *Partial pressure [atm] of CO_2 and H_2S for stream B and F.*

	Stream B	*Stream F*
Partial pressure$_{CO_2}[atm]$	0.17	0.17
Partial pressure$_{H_2S}[atm]$	0.14	0.13

From the given values a ratio between carbon dioxide and hydrogen sulfide was calculated

which gave an indication of which type of sour, mixed or sweet corrosion that is dominating in the amine recovery system of the SynSat unit. It is known that for carbon steel material, a CO_2/H_2S ratio < 20 gives a sour corrosion dominance, a ratio of 20 - 500 a mixed regime of sweet and sour corrosion and a ratio > 500 gives a sweet corrosion dominance. In Table 4.16 calculated ratios for the both streams are presented. The calculations show a very low ratio for both streams with all of them being < 20, resulting in a dominating sour corrosion.

Table 4.16: *CO_2/H_2S ratio for stream B and F.*

	Stream B	*Stream F*
CO_2/H_2S ratio	1.22	1.31

Both ratios showed to be smaller than initially expected with a low composition of CO_2 in particular. With such low values as provided for the streams, the effect of CO_2 can be seen as limited in comparison with the SynSat unit before the revamp when CO_2 was not present.

Calculating the CO_2/H_2S ratio some assumptions has to be done in order to use the method as described in Section 2.6.4. What might be the most important assumption in this case is the temperature and phase formation of FeS. The model is used at temperatures up to 100 °C and is assuming both iron carbide and mackinawite present in the system. This complicates matters when it comes to the amine recovery system in the SynSat unit. Here the lowest temperature reached is 118 °C. Therefore both streams (B and F) will probably have a formation of pyrrhotite, troilite or other forms of more stable iron sulfide or chromium sulfide, thereby increasing the ratio for sweet corrosion to > 2500. Our calculated CO_2/H_2S ratios have values < 2 which gives a clear indication of corrosion type, but it is very important to understand that this method only gives a broad indication of occurring type of corrosion. This due to the sensitivity of thermodynamic data put in to the method. Therefore simulations or other calculations for formation of iron carbide and iron sulfide is to prefer such as theoretical or practical corrosion prediction models for sour corrosion.

During investigation of the possibilities of finding useful and adaptable prediction models for sour corrosion, very little information has been found published in reports and articles. Mainly due to the complicated formation of protective corrosion film layers of iron sulfide. Therefore no corrosion prediction model has been found of interest in this project and is therefore left open for further investigations.

5 Conclusions

The analyzed LAGO samples with mixtures of 5, 10, 15 and 100 wt% rapeseed oil respectively, at 290, 310 and 330 °C was found to yield no risk of corrosion to the current stainless steel material alloy 321. The performed tests showed that an increase of TAN was found to dependent more on the different temperatures analyzed than between the mixtures of rapeseed oil. It can therefore be concluded that co-processing LAGO with rapeseed oil up to 100 wt% of rapeseed oil at 330 °C is of no great risk of corrosion at the SynSat unit in Preems refinery in Lysekil. This due to the low decomposition of triglycerides to free fatty acids which is related to steel corrosion.

The effect of a hydrogen atmosphere was proven to be of great importance with respect to decomposition of triglycerides into free fatty acids. The results of this master thesis showed that the presence of hydrogen gas gave a significant lower TAN value at the investigated mixtures and temperatures of 290, 310 and 330 °C.

It was found that the planned first injection point of wash water is necessary in order to avoid deposition of ammonium chloride salt which later can cause fouling and corrosion, mainly in the pipe materials of heat exchangers and/or air coolers. Ammonium bisulfide which also was investigated showed no risk of salt deposition at the current stream parameters.

Sour corrosion was found to be dominating at the amine recovery system of the SynSat unit. Two of the streams showed to have liquid water phase which can cause sour corrosion to occur. The corrosion type and the rate of corrosion was however not found due to little information in published literature with respect to the sour corrosion mechanism. It is therefore left open for further studies and investigations.

Bibliography

[1] Gong S, Shinozaki A, Shi M, Qian E.W. Hydrotreating of Jatropha Oil over Alumina Based Catalyst. *Energy Fuels* 2012; 26:4: p. 2394-2399. https://doi.org/10.1021/ef300047a

[2] Sotelo-Boyás R, Liu Y, Minowa T. Renewable Diesel production from the Hyrdotreating of Rapeseed Oil with Pt/Zeolite and NiMo/Al2O3 Catalysts. *Ind. Eng. Chem. Res.* 2011; 46:2: p. 2791-2799. https://doi.org/10.1021/ie100824d

[3] Baig A, Paszti M, Ng F.T.T. A simple and green analytical method for acid number analysis of biodiesel and biodiesel blends based on potentiometric technique. *Fuel* 2013; 104: p. 426-432. https://doi.org/10.1016/j.fuel.2012.06.012

[4] Chen S. Green Oil Production by Hydroprocessing. *International Journal of Clean Coal and Energy* 2012; 1:4: p. 43-55. http://dx.doi.org/10.4236/ijcce.2012.14005

[5] Valencia D, García-Cruz I, Uc V.H, Ramírez-Verduzco L.F, Amezcua-Allieri M.A, Aburto J. Unravelling the chemical reactions of fatty acids and triglycerides under hydrodeoxygenation conditions based on a comprehensive thermodynamic analysis. *Biomass and Bioenergy* 2018; 112: p. 37-44. https://doi.org/10.1016/j.biombioe.2018.02.014

[6] Zeuthen P, Rasmussen H. Future fuel - the challenges associated with renewable diesel hydrotreating. *Digital Refining* 2016. Available from www.digitalrefining.com/article/1001237. Accessed the 10th of august 2019.

[7] Melero J.A, Calleja G, Garcia A, Clavero M, Hernandez E.A, Miravalles R, Galindo T. Storage stability and corrosion studies of renewable raw materials and petrol mixtures: A key for their co-processing in refinery units. *Fuel* 2010; 89:3: p. 554-562. https://doi.org/10.1016/j.fuel.2009.09.026

[8] Brady M.P, Keiser J.R, Leonard D.N, Zacher A.H, Bryden K.J, Weatherbee G.D. Corrosion of stainless steels in the riser during co-processing of bio-oils in a fluid catalytic cracking pilot plant. *Fuel process. technol.* 2017; 159: p. 187-199. https://doi.org/10.1016/j.fuproc.2017.01.041

[9] The Hendrix Group, Materials and Corrosion Engineers. Available from http://hghouston.com/resources/special-corrosion-topics/ammonium-chloride. Accessed 2nd of april 2020.

[10] Otzisk B, Margi F, Achten J, Halsberghe S. Preventing ammonium salt fouling and corrosion. *Digital Refining* 2018. Available from www.digitalrefining.com/article/1001460. Accessed the 20th of april 2020.

[11] Renpu W. (2011): p. 630-636. Advanced Well Completion Engineering (3rd Edition). Waltham, Maine, United States. Gulf Professional Publishing.

[12] Loganathan S. Biohydro-fined diesel (BHD) and biodiesel (BOB) production process and property review. *Innovations in Fuel Economy and Sustainable Road Transport* 2011; p. 97-107. https://doi.org/10.1533/9780857095879.2.97

[13] Patrick B.N. Understanding Naphthenic Acid Corrosion in Refinery Settings. *University of California, Berkeley* 2015.

[14] Chernova A, Gubaev R, Mazin P, Goryunova S, Demurin Y, Gorlova L, Vanushkina A, Mair W, Anikanov N, Martynova E, Goryunov D, Garkusha S, Mukhina Z, Khaytovich P. UPLC-MS Triglyceride Profiling in Sunflower and Rapeseed Seeds. *Biomolecules* 2019; 9:1: p. 1-10. https://doi.org/10.3390/biom9010009

[15] McVetty P. Duncan R.W. (2015): p. 133-156. Canola, Rapeseed, and Mustard: For Biofuels and Bioproducts. Boston, Maine, United Stated: Springer.

[16] National Edible Oil Distributors Association. Chemistry of Oil and Fats. Available from www.neoda.org.uk/oils-fats-information . Accessed 14th of august 2019.

[17] Brostrom M, Kassman H, Helgesson A, Berg M, Andersson C, Backman R, Nordin A. Sulfation of corrosive alkali chlorides by ammonium sulfate in a biomass fired CFB boiler. *Fuel processing technology* 2007; 88:11-12: p. 1171-1177. https://doi.org/10.1016/j.fuproc.2007.06.023

[18] Gupta M.K. (2017): p. 7-25. Practical Guide to Vegetable Oil Processing (2nd Edition). Lynnwood, Texas, United States: AOCS Press. Published by Elsevier Inc. https://doi.org/10.1016/B978-1-63067-050-4.00002-7

[19] Przybylski R. Canola Oil Physical and Chemical Properties. Available from https://fr.canolacouncil.org/media/515239/canola_oil_physical_chemical_properties_1.pdf Accessed 8th of october 2019.

[20] Schillmoller C.M. Selection and use of stainless steels and nickel-bearing alloys in organic acids. *Nickel Development Institute*. No. 10 063. Available from https://www.valve-world.net/pdf/10063.pdf. Accessed 8th of november 2019.

[21] U.S National Library of Medicine. Available from www.pubchem.ncbi.nlm.nih.gov/compound/445639. Accessed 1st of november 2019.

[22] U.S National Library of Medicine. Available from

www.pubchem.ncbi.nlm.nih.gov/compound/5280450. Accessed 1st of november 2019.

[23] U.S National Library of Medicine. Available from www.pubchem.ncbi.nlm.nih.gov/compound/5280934. Accessed 1st of november 2019.

[24] Palanisamy S. Co-processing Fat-rich Material into Diesel Fuel. *Chalmers Univeristy of Technology*, Gothenburg 2013.

[25] Nickel Development Institute. The role of stainless steels in petroleum refining. Available from https://www.nickelinstitute.org/media/1781/roleofstainlesssteelinpetroleumrefining_9021_.pdf. Accessed 1st of november 2019.

[26] Yamaguchi N. (2003). Hydrodesulfurization Technologies and Costs. Mexico City, Mexico. Trans Energy Associates, William and Flora Hewlett Foundation Sulfur Workshop. Accessed november 14th of november 2019.

[27] Spraying Systemas Co. Optimizing quill and injector performance in refinery operations. Available from https://www.spray.com/literature_pdfs/wp109_optimizing_inj_quill_perf.pdf. Accessed the 10th of august 2019.

[28] Lira-Galeana C, Hammami A. Wax precipitation from petroleum fluids: a review. *Devlopment in Petroleum Science* 2000; 40:B: p. 557-608. https://doi.org/10.1016/S0376-7361(09)70292-4

[29] Bacha J, Freel J, Gibbs A, Hemighaus G, Hoekman K, Horn J, Gibbs A, Ingham M, Jossens L, Kohler D, Lesnii D, McGeehan J, Nikanjam M, Olsen E, Organ R, Scott B, Sztenderowicz M, Tiedemann A, Walker C, Lind J, Jones J, Scott D, Mills J. Diesel Fuels Technical Review. *Chevron Corporation.* San Ramon, CA, 2007. Available from https://www.chevron.com/-/media/chevron/operations/documents/diesel-fuel-tech-review.pdf. Accessed 8th of november 2019.

[30] Šimáček P, Kubička D. Hydrocracking of petroleum vacuum distillate containing rapeseed oil: Evaluation of diesel fuel. *Fuel* 2010; 89:7: p. 1508-1513. www.doi.org/10.1016/j.fuel.2009.09.029

[31] Ameen A, Tazli Azizan M, Yusup S, Ramli A, Yasir M. Catalytic hydrodeoxygenation of triglycerides: An approach to clean diesel fuel production. *Renewable and Sustainable Energy Reviews* 2017; 80: 1072-1088. https: https://doi.org/10.1016/j.rser.2017.05.268

[32] Sugami Y, Minami E, Saka S. Renewable diesel production from rapeseed oil with hydrothermal hydrogenation and subsequent decarboxylation. *Fuel* 2016; 166: p. 376-381. https://doi.org/10.1016/j.fuel.2015.10.117

[33] Walendziewski J, Stolarski M, Łużny R, Klimek B. Hydroprocessing of light gas oil - rape oil mixtures. *Fuel Processing Technology* 2009; 90:5: p. 686-691. https://doi.org/10.1016/j.fuproc.2008.12.006

[34] Mortensen P.M, Grunwaldt J.-D, Jensen P.A, Knudsen K.G, Jensen A.D. A review of catalytic upgrading of bio-oil to engine fuels. *Applied Catalysis A: General* 2011; 407:1-2: p. 1-19. https://doi.org/10.1016/j.apcata.2011.08.046

[35] Knothe G. Dependence of biodiesel fuel properties on the structure of fatty acid alkyl esters. *Fuel Processing Technology* 2005; 86:10: p. 1059-1070. https://doi.org/10.1016/j.fuproc.2004.11.002

[36] Vallero D.A. (2010) p. 99-165. Environmental Biotechnology, A Biosystems Approach. Amsterdam, The Netherlands: Academic Press. https://doi.org/10.1016/C2009-0-01984-9

[37] Meier H.F, Wiggers V.R, Zonta G.R, Scharf D.R, Simionatto E.L, Ender L. A kinetic model for thermal cracking of waste cooking oil based on chemical lumps. *Fuel* 2015; 144: p. 50-59. https://doi.org/10.1016/j.fuel.2014.12.020. Corrigendum in *Fuel* 2015; 157: p. 299. https://doi.org/10.1016/j.fuel.2015.05.001.

[38] Makhlouf A.S.H, Herrera V, Muñoz M. (2018): p. 107-122. Handbook of Materials Failure Analysis - With case Studies from the Construction Industries. Elsevier. https://app.knovel.com/hotlink/toc/id:kpHMFAWCS1/handbook-materials-failure/handbook-materials-failure

[39] Coker K. (2015): p. 1209-1241. Ludwig's Applied Process Design for Chemical and Petrochemical Plants (4th Edition). Houston, Texas, United States: Gulf Professional Publishing. http:// 10.1016/B978-0-7506-8524-5.00022-7

[40] Jones D.A. (1996): p. 8, 50, 116-121. Principles and prevention of corrosion (2nd Edition). Upper Saddle River, New Jersey, United States: Simon Schuster/ A viacom Company. ISBN: 0-13-359993-0

[41] Chang C-M, Hsieh C-C. Lin C-M, Chen J-H, Fan C-M, Wu W. Effect of carbon content on microstructure and corrosion behaviour of hypereutectic Fe-Cr-C claddings. *Materials Chemistry and Physics* 2010; 123: p. 241-246. https://doi.org/10.1016/j.matchemphys.2010.04.003

[42] Alvisi P.P, de Freitas Cunha Lins V. Acid salt corrosion in a hydrotreatment plant of a petroleum refinery. *Engineering Failure Analysis* 2008; 15: p. 1035-1041.

[43] Akpanyung K.V. An Overview of Ammonium Chloride (NH_4Cl) Corrosion in the Refining Unit. *J. Phys.: Conf* 2019; Ser. 1379 022089.

[44] Petersen P.R, De Jong A, Sigmon J.L, Minyard W.F. (2001). Impact of Ammonium Chloride Salt Deposition on Refinery Operations. CORROSION 2001 (p. no. 01540). Houston, Texas, Unites States: NACE International. Available from https://www.onepetro.org/conference-paper/NACE-01540.

Accessed 2nd of april 2020.

[45] Mahajanam S, Addington F, Barba A, Copple B, Cuenca N, Folse J, Mao Y, White J, Williamson K. (2017). Ammonium Chloride Corrosion in the Refining Industry. CORROSION 2017 (p. no. 9574). New Orleans, Louisiana, Unites States: NACE International. Available from https://www.onepetro.org/conference-paper/NACE-2017-9574. Accessed 2nd of april 2020.

[46] Baboian R. (2005): p. 425-433. Corrosion Tests and Standards: Application and Interpretation (2nd Edition). Baltimore, Maryland, United States: ASTM International.

[47] Smith S.N, Pacheco J.L. Prediction of Corrosion in Slightly Sour Environments. CORROSION 2002 (p. no. 02241). Denver, Colorado, Unites States: NACE International. Available from https://www.researchgate.net/publication/261522119_Prediction_of_Corrosion_in_Slightly_Sour_Environments5. Accessed 5th of february 2020.

[48] Rebak R.B, Perez T.E. (2017). Effect of Carbon Dioxide and Hydrogen Sulfide on the Localized Corrosion of Carbon Steels and Corrosion Resistance Alloys. CORROSION 2017 (p. no. 8933). New Orleans, Louisiana, Unites States: NACE International. Available from https://www.onepetro.org/conference-paper/NACE-2017-8933. Accessed 19th of february 2020.

[49] Smith S.N. The Carbon Dioxide/Hydrogen Sulfide Ratio - Use and Relevance. *Materials Performance* 2015; 54:5.

[50] Groysman A. (2017): p. 50 - 53. Corrosion Problems and Solutions in Oil Refining and Petrochemical industry. Cham, Switzerland: Springer International Publishing AG.

[51] El-Sherik A.M. (2017): p. 113-190. Trends in Oil and Gas Corrosion Research and Technologies: Production and Transmission (1st Edition). Duxford, United Kingdom. Woodhead Publishing.

[52] Tait W.S. (2018): p. 584-600. Handbook of Environmental Degradation of Materials (3rd Edition). Oxford, United Kingdom. Elsevier Inc.

[53] Speight J.G. (2014): p. 1-55. High Acid Crudes. Oxford, United Kingdom: Gulf Professional Publishing, Elsevier.

[54] Smith S.N. A proposed Mechanism for Corrosion in slightly Sour Oil and Gas Production. International Corrosion Congress (1993), (Issue no. 385) Houston, Texas, United States. Available from https://www.researchgate.net/publication/261174874. Accessed 19th of february 2020.

[55] Snow D.A. (2003): p. 33-1-33-25. Plant Engineer's Reference Book (2nd Edition). Great Britain. Reed Educational and Professional Publishing Ltd.

[56] Sun W, Nešić S. A Mechanistic Model of Uniform Hydrogen Sulfide/Carbon Dioxide Corrosion of Mild Steel. *CORROSION* 2009; 65(5): p. 291-307. https://doi.org/10.5006/1.3319134

[57] Wallaert E, Depover T, De Graeve I, Verbeken K. FeS Corrosion Products and Hydrogen Uptake in a Sour Environment for Quenched Tempered Steel. *Metals* 2018; 8(1): 62. https://doi.org/10.3390/met8010062

[58] Anderko A, Young R.D. Simulation of CO_2/H_2S Corrosion Using Thermodynamic and Electrochemical Models. CORROSION 1999. San Antonio, Texas, United States: NACE International.

[59] Park L.K-E, Liu J, Yiacoumi S, Borole A.P, Tsouris C. Contribution of acidic components to the total acid number (TAN) of bio-oil. *Fuel* 2007;200: p. 171-181. https://doi.org/10.1016/j.fuel.2017.03.022

[60] Speight J.G. (2017): p. 254. Handbook of Petroleum Refining. Boca Raton, Florida, United States: CRC Press, Taylor and Francis Group.

[61] Gudmundsson J.S. (2017): p. 199-208. Flow Assurance in Oil and Gas Production. Leiden, The Netherlands: CRC Press, Taylor and Francis Group.

[62] Sandmeyer Steel Company. Philadelphia, Pennsylvania, United States. Specification Sheet: Alloy 321/321 H. Available from https://www.sandmeyersteel.com/images/Alloy321-SpecSheet.pdf. Accessed 11th of september 2019.

[63] Damstahl. Malmö, Sweden. Available from https://www.damstahl.se/globalassets/downloads-130x185/sverige/produktkatalog/12b_technical_info_eng.pdf. Accessed 6th of december 2019.

[64] Encyclopedia Britannica, Inc. Chicago, Illinois, United States. Stainless Steel Matallurgy. Available from https://www.britannica.com/technology/stainless-steelref137957. Accessed 10th of september 2019.

[65] McGuire, M. F. (2008): p. 69-90. Stainless Steels for Design Engineers. Materials Park, Ohio, United States: ASM International. ISBN-13: 978-0-87170-717-8

[66] McGuire, M.F. (2001) p. 406-410. Encyclopedia of Materials: Science and Technology (2nd Edition). Fox Chapel, Pennsylvania, United States: Elsevier Science Technology. https://doi.org/10.1016/B0-08-043152-6/00081-4

[67] Nickel Development Institute. Available from https://www.nickelinstitute.org/about-nickel/stainless-steel/. Accessed 1st of november 2019.

[68] Gallo G, Edmondson J. (2008). The Effect of Molybdenum On Stainless Steels And Naphthenic Acid Corrosion Resistance. CORROSION 2008 (p.1-13). New Orleans, Louisiana, Unites States: NACE International. Available from https://www.onepetro.org/conference-paper/NACE-08555. Accessed 1st of november 2019.

[69] Sandmeyer Steel Company. Philadelphia, Pennsylvania, United States. Specification Sheet: Alloy 316. Available from https://www.sandmeyersteel.com/316-316L.html. Accessed 6th of december 2019.

[70] Sandmeyer Steel Company. Philadelphia, Pennsylvania, United States. Specification Sheet: Alloy 317L. Available from https://www.sandmeyersteel.com/images/Alloy317L-SpecSheet.pdf. Accessed 11th of september 2019.

[71] Research Institutes of Sweden. Available from https://www.ri.se/en/better-future-and-those-who-take-us-there. Accessed 17th of october 2019.

[72] ASTM International. Standard Test Method for Acid Number of Petroleum Products by Potentiometric Titration, ASTM D664-18e2. 2006.

[73] British Broadcasting Corporation. Available from https://www.bbc.co.uk/bitesize/guides/zqxyjty/revision/4. Accessed 28th of april 2020.

[74] The Hendrix Group, Materials and Corrosion Engineers. Available from http://hghouston.com/resources/special-corrosion-topics/ammonium-bisulfide. Accessed 2nd of april 2020.

[75] Mörtstedt S.E, Hellsten G (2012): p. 36. Data och Diagram (6th edition). Stockholm, Sweden: Liber AB.

[76] American Petroleum Institute. API Recommended Practice 581, Risk-Based Inspection Technology (3rd edition). Year of Issue: 2016.

A Appendices

A.1 Appendix I

In Figure A.1 the work procedure when heat treating the used samples in this report i shown. A total of 160 minutes was set to assure steady state before the first sample of 30ml was collected. A total of three samples per blend and temperature were gathered before changing the wt% of rapeseed oil. This process was repeated until all three samples for the desired temperature were collected and then a new cycle started, repeating the procedure. Sample 4, 8 and 12 all with 100 wt% of rapeseed oil was heat treated lastly in order to avoid coke on the silicone carbide inside the column.

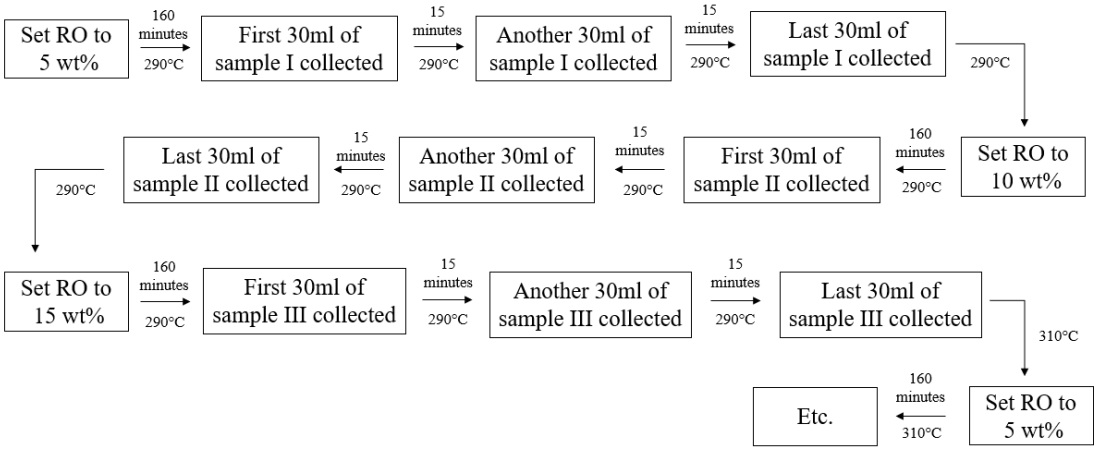

Figure A.1: *Worksheet of time over the heating treatment at RISE.*

A.2 Appendix II

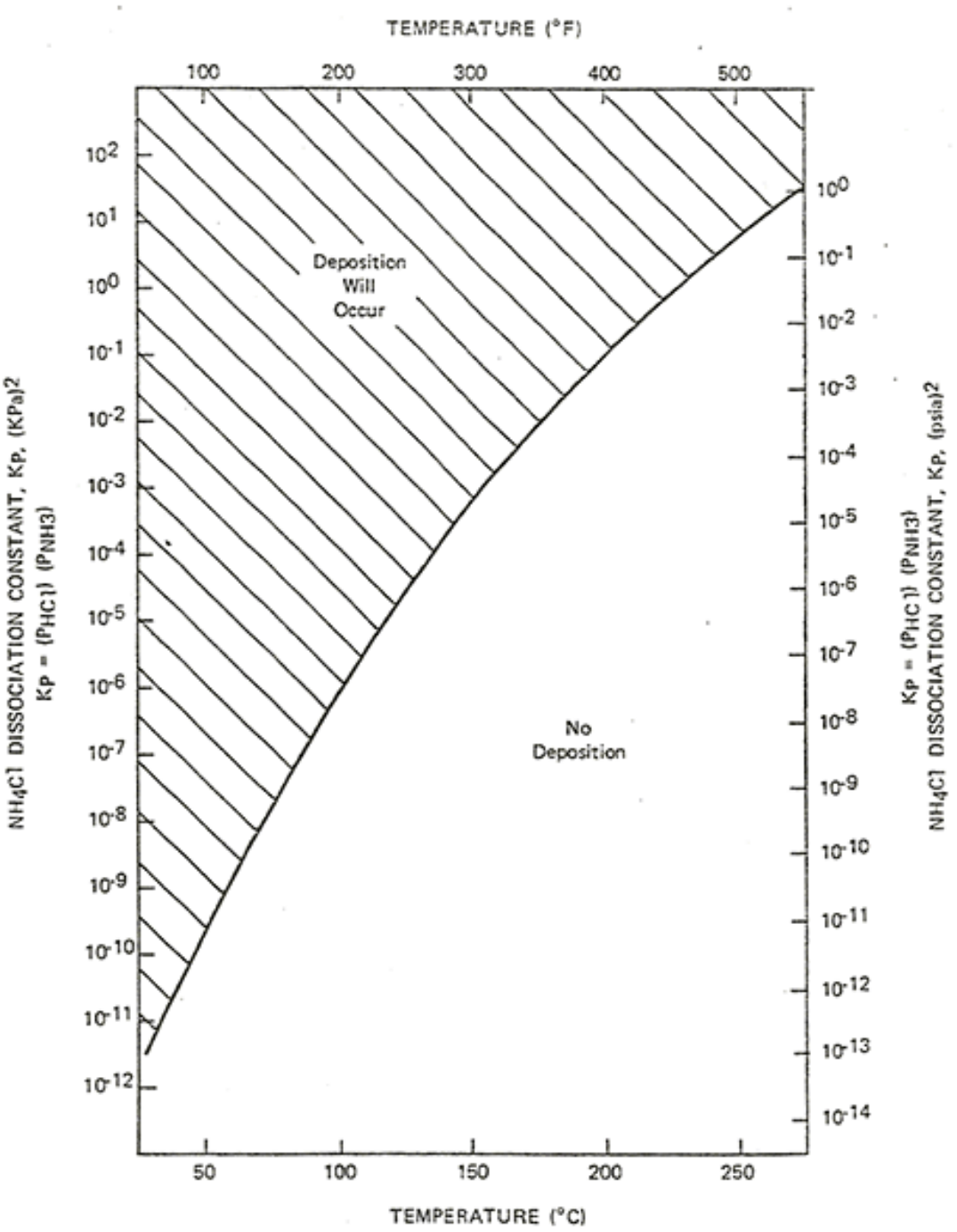

Figure A.2: *Diagram over deposition of NH_4Cl salt.* [9]

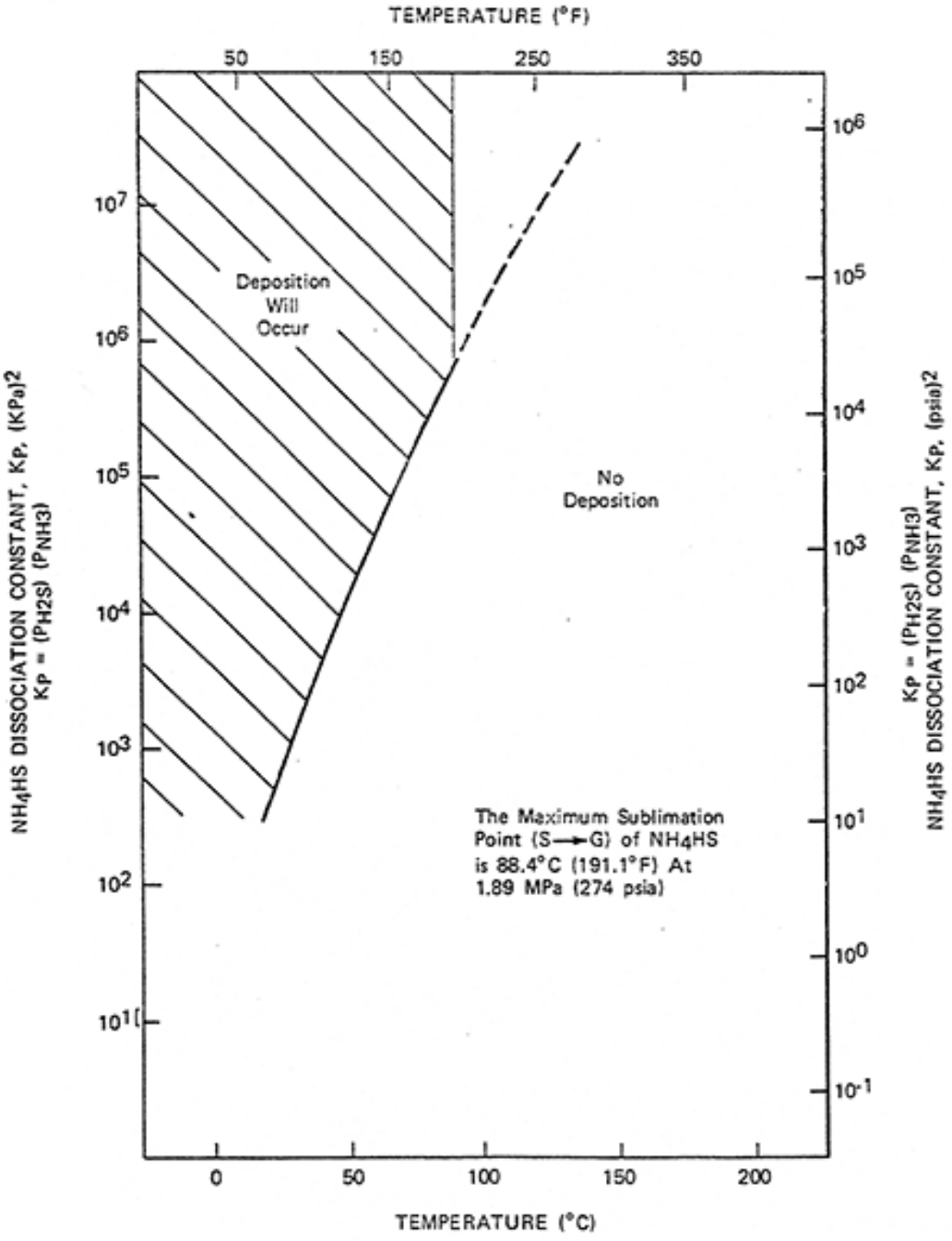

Figure A.3: *Diagram over deposition of NH_4HS salt.* [74]